



HAL
open science

Low-frequency amplification of propeller tonal noise due to the scattering by a compact rigid cylinder

Elina Cros, Michel Roger, Gilles Serre

► To cite this version:

Elina Cros, Michel Roger, Gilles Serre. Low-frequency amplification of propeller tonal noise due to the scattering by a compact rigid cylinder. *Journal of Sound and Vibration*, 2023, 546, pp.117450. 10.1016/j.jsv.2022.117450 . hal-04741282

HAL Id: hal-04741282

<https://hal.science/hal-04741282v1>

Submitted on 17 Oct 2024

HAL is a multi-disciplinary open access archive for the deposit and dissemination of scientific research documents, whether they are published or not. The documents may come from teaching and research institutions in France or abroad, or from public or private research centers.

L'archive ouverte pluridisciplinaire **HAL**, est destinée au dépôt et à la diffusion de documents scientifiques de niveau recherche, publiés ou non, émanant des établissements d'enseignement et de recherche français ou étrangers, des laboratoires publics ou privés.

Low-frequency amplification of propeller tonal noise due to the scattering by a compact rigid cylinder

Elina Cros^{a,b,*}, Michel Roger^a, Gilles Serre^b

^a*Univ Lyon, Ecole Centrale de Lyon, CNRS, Univ Claude Bernard Lyon 1, INSA Lyon, LMFA, UMR5509, 69130, Écully, France*

^b*Naval Group Research, 199 avenue Pierre Gilles de Gennes, 83190 Ollioules, France*

Abstract

The present work addresses the scattering of the tonal noise of a low-speed propeller by a rigid cylinder, as a generic configuration representative of installed marine propellers. Both propeller and cylinder axes are parallel to each other. The diameters of the propeller and of the cylinder are much smaller than the acoustic wavelengths, as well as the propeller-cylinder distance. This corresponds to a compact regime of diffraction. Only the hydrodynamic tonal noise of the propeller at the first multiples of the blade-passing frequency is considered, assuming rigid blades, in a two-dimensional formulation. The direct and scattered sound fields are expressed in terms of spinning modes, with respect to the propeller and cylinder axes, respectively. Use is made of the exact Green's function of the cylinder for the Helmholtz equation. The modes of orders ± 1 are found the only efficient ones in the direct field, whereas higher-order modes rapidly decay. Yet, in the presence of the cylinder, higher-order modes are scattered into the contra-rotating mode of order 1 in the reference frame of the cylinder, with a strong amplification. A simple experiment, performed in air but with Helmholtz numbers typical of marine applications, confirms these results as key features of the asymptotic Green's function of the cylinder. The same modal behavior is reproduced as closed-form simple expressions from a low-frequency approximation of the Green's function. The results show that

*Corresponding author

Email address: `elina.cros@ec-lyon.fr` (Elina Cros)

the installation effect is crucial for the tonal noise of marine propellers at very low frequencies.

Keywords: Marine propeller noise, Spinning modes, Analytical modelling, Diffraction

Nomenclature

Italic symbols

	a	cylinder radius
	A_n	modal amplitude in array processing
5	B	blade number
	c_0	sound speed
	D	distance from cylinder axis to propeller axis
	e_X, e_Y, e_Z	unit vectors of main directions
	\mathbf{F}	point-dipole force
10	\mathbf{F}_s	point-dipole force harmonic
	$F_s^{A,T,R}$	Fourier coefficients of axial, tangential and radial forces
	G	Green's function for the Helmholtz equation
	G_0	free-field Green's function
	G_{0as}	asymptotic free-field Green's function
15	G_1	2-D cylinder Green's function
	G_{1as}	asymptotic cylinder Green's function
	L	distance from cylinder edge to propeller axis
	$J_m, H_m^{(1)}$	Bessel and Hankel functions of the first kind
	k	acoustic wavenumber
20	m	summation index, mode order in array processing
	M	tangential Mach number
	M_n	phase tangential Mach number
	n	spinning mode order (number of lobes)
	p_{0as}, p_{1as}	free-field and scattered pressures in asymptotic regime
25	$p_{\mu B}$	complex acoustic pressure at a BPF harmonic

	p_{ar}	free-field pressure expanded as spinning modes
	p_m	sound-pressure modal amplitude
	r_ϕ	observer distance to a source-mode point
	r, R_0	circle radius
30	R	observer distance to origin
	s	blade loading harmonic order
	$\mathbf{x} = (r_x, \theta_x)$	observer position
	$\mathbf{y} = (r_y, \theta_y)$	source position
	(x_1, x_2)	components of \mathbf{x} in Cartesian coordinate system
35	(y_1, y_2)	components of \mathbf{y} in Cartesian coordinate system

Greek symbols

	λ	wavelength
	μ	BPF harmonic order
	Θ	observer angle from axis
40	ζ	rotor-blade force-inclination angle
	ω	angular frequency
	Ω	rotational speed
	ξ	observer angle in polar coordinates
	Φ	polar observer angle
45	ϕ	polar angle of source-mode point

Abbreviations

	BLH	blade loading harmonic
	BPF	blade passing frequency
	PSD	power spectral densities
50	SPL	sound pressure level

1. Introduction

Sound generation and propagation from ships in water is a matter of concern for both the acoustic discretion of ships and the protection of aquatic wild life.

It involves complex physical aspects, especially dealing with propeller-associated
55 sound-generating mechanisms. Firstly, structure-borne noise is emitted because
mechanical vibrations are transmitted to the hull through the driving shaft.
Secondly, the propellers are known to generate hydrodynamic noise. The latter
is generally the most significant contribution to the total noise. This is why the
design of modern marine propellers has to combine better hydrodynamic effi-
60 ciency and reduced emitted sound. For this, the involved mechanisms must be
identified and dedicated prediction models that could be introduced at the early
stages of optimization processes are needed. The most crucial aspects of marine
propeller noise are the so-called installation effects, which are twofold. Firstly,
the propellers are always mounted in the rear part of the ship hull, therefore
65 they are partly embedded in a non-homogeneous and turbulent wake and/or
interact with the turbulent boundary layer developing along the whole length
of the hull. Random and periodic fluctuations are induced on the blades, lead-
ing to increased, respectively broadband and tonal, acoustic signatures, when
compared to what the isolated propeller would radiate. This is referred to as
70 the hydrodynamic installation effect. In particular, stationary azimuthal dis-
tortions, defined as deviations from pure axisymmetry of the flow around the
propeller axis, generate additional tonal noise.

Secondly, the mounting of propellers in close vicinity of the hull makes the
sound radiated from the blades scattered, in such a way that the basic radiating
75 properties of the sources are strongly modified. This is especially pronounced
for the sources of the tonal noise, structured by interfering isolated-blade con-
tributions: the vicinity of the hull introduces imbalance in the interference. As
a result, the noise of an installed propeller can dramatically differ from what
the free-field noise would be, even considering the same sources. This second
80 effect, addressed in the present work, is called the acoustic installation effect.

Both installation effects are usually investigated independently. The noise
that would be radiated by a propeller in free field but with the real flow dis-
tortions, thus the true sources, can be predicted relying on Ffowcs Williams
& Hawking's formulation of the acoustic analogy [1, 2, 3], initially developed

85 for aeronautical applications. Indeed, the same formal background holds for
air and water, basic differences being in the characteristic Mach and Reynolds
numbers. The only specific feature of marine propellers is the cavitation, known
as a dominant source of noise in many configurations. But cavitation noise is
discarded from the present analysis. In the analogy, the rotating blades and
90 their accompanying unsteady flows are formally replaced by equivalent sources
that are assumed to radiate in a uniform and stagnant unbounded medium. The
associated wave equation is therefore usually solved with the standard free-field
Green's function. Dimensional analysis indicates that, within this framework
and at very low Mach numbers, the major source of noise is the passage of the
95 propeller blades through the distortions, which generates fluctuating forces on
the blades acting as equivalent acoustic dipoles [3]. This defines the so-called un-
steady loading noise. The averaged force on the blades, which would be the only
remaining hydrodynamic force in absence of distortion, is responsible for the
steady-loading noise. Rotating blades also generate thickness noise. The latter
100 can be modeled again from equivalent dipoles, according to Isom's formulation
(see for instance Farassat [4]). Therefore, rotating dipoles are considered here
as the only required generic background for the description of marine propeller
noise. As long as the tonal noise at harmonics of the Blade-Passing Frequency
(BPF) is considered, each tone is a sum of elementary patterns called spinning
105 radiation modes. This notion is reminded in the paper. A mode is a diverging
pressure wave, combined with an azimuthally periodic pattern spinning at some
phase speed, and forced by the dipole source strength.

In the presence of surrounding surfaces, a tailored Green's function must
be used or the wave equation of the analogy solved numerically with additional
110 boundary conditions imposed on the surfaces, depending on the geometry of the
latter. This has been the basis of hybrid methods developed in hydroacoustics to
estimate the noise nearby the hull of a ship [5, 6]. In the present work, diffraction
is addressed assuming a rigid cylinder instead of a true hull geometry (Fig. 1),
in order to highlight key mechanisms with a simple mathematical background.
115 The exact tailored Green's function of the cylinder for the Helmholtz equation

is used to this end, the problem being stated in the frequency domain. Indeed, diffraction is a matter of compared source-to-obstacle distance and acoustic wavelength. The consequence is that the amount of scattering differs for all angular positions of a blade element seen as source along its circular path.
120 This causes imbalance in the partial cancellations which determine the radiation efficiency of a spinning mode. In order to take this exactly into account in the study, each spinning mode is reproduced with an equivalent circular distribution of stationary phased dipoles, referred to as a source-mode [7, 8].

Installed marine propellers correspond to very compact configurations, in
125 the sense that both the blade-tip radius and the distance to the ship hull are much smaller than the emitted acoustic wavelengths. This is especially true in the very-low frequency range corresponding to the first harmonics of the BPF (Blade-Passing Frequency, defined as the rotational frequency $\Omega/(2\pi)$ multiplied by the number of blades B), investigated in the present work. Typically, for a
130 BPF of 30 Hz and a sound speed of 1500 m/s, the Helmholtz number built of some characteristic length Λ remains below 0.1 for values of Λ up to 8 m. This confirms that the propeller-hull distance, and to some extent also the region including the blades and the hull cross-section, is acoustically compact. Therefore, the source-modes must be assumed in the very vicinity of the cylinder
135 to be representative of a marine application. A compact approximation of the Green's function is justified in such cases, in the sense introduced by Howe [9]. This particular regime is crucial because it is known to produce a more or less pronounced amplification of the sound from sources of high equivalent polar orders. The amplification has been reported in similar studies, based on
140 asymptotic analyses performed on exact Green's functions [10, 11], for sources approaching the edge of a rigid half-plane.

The aforementioned context motivated the authors in addressing specifically the compact regime of the scattering of a source-mode by a rigid cylinder. The configuration is understood as a generic one, representative of a marine propeller
145 installed close to a ship hull. It is addressed here with a two-dimensional model to provide a first insight into the underlying physics. Because the main scat-

tering features involve the normal distances from the sources to the cylinder, three-dimensional refinements would not question the main observed trends. They will be the matter for a future extension of the work. In fact, a dedicated experiment has also been carried out in air, in an anechoic room, in order to validate the relevance of the two-dimensional model. The setup includes a small-size three-bladed propeller operated close to a rigid cylinder, with ratios of wavelengths to dimensions representative of marine applications. The study is aimed at pointing out that the diffraction is able to generate much higher sound than the direct source-mode radiation in free field. Some theoretical background of tonal rotating-blade noise for compact blades and the notion of associated source-modes are introduced in section 2. The analytical expressions of the scattered sound field based on the two-dimensional tailored Green's function of the rigid cylinder for the Helmholtz equation are derived in section 3. The developments specific to the asymptotic regime for a far-field observer and arbitrary source-modes are detailed in section 4. The aim is to highlight the amplification caused by cylinder scattering at very low frequencies. The effects of the source-to-cylinder distance and of other key parameters are discussed. The accompanying experiment is described in section 5, where the main results are discussed, confirming the amplification mechanism. Finally, the effect of the hub of a propeller is shortly addressed in section 6.

2. Free-Field Tonal Noise Formulation

Before addressing the theoretical model of sound scattering by a rigid cylinder, elementary expressions for the acoustic pressure radiated by a propeller in the far field are reviewed in this section. The fluid motion relative to the reference frame of the propeller is neglected when describing sound propagation, in view of the negligibly small Mach numbers. Yet local azimuthal flow distortions are indirectly accounted for by the associated blade-loading harmonics. The far-field expressions are considered only as a reference for the analysis of the modal properties of the radiated field.

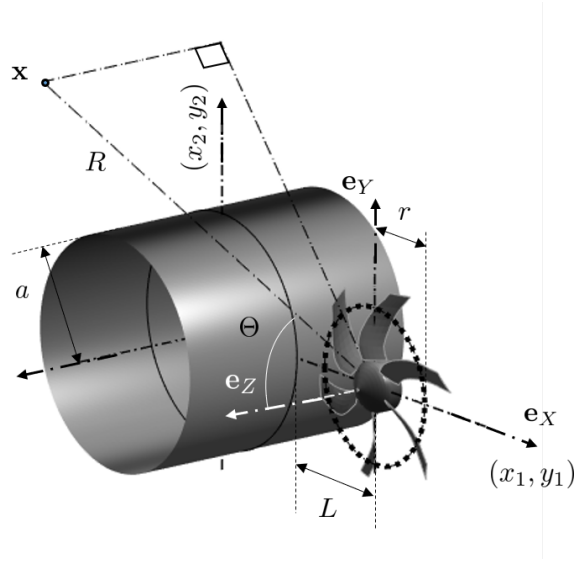


Figure 1: Propeller and cylinder reference frames, with spherical coordinates for the three-dimensional formulation of propeller noise. Discretized source-mode of radius r featured by the circular array of dots. Subsequent developments refer to the rotor-disk plane ($\mathbf{e}_X, \mathbf{e}_Y$).

2.1. Rotating-Blade Noise Formulation

Tonal rotor noise is usually formulated in the frequency domain in the far-field, relying on Ffowcs Williams & Hawkings' formulation of the acoustic analogy [1, 2]. The mathematical solution is reminded in this section as a back-
 180 ground for the present developments, assuming a single acoustically compact blade element rotating at constant angular speed Ω on the circle of radius r in a quiescent propagation medium. Details can also be found in references [12, 13]. With the conventional notation $e^{-i\omega t}$ for monochromatic waves of angular frequency ω , the complex-valued amplitude of the far-field acoustic pressure at the
 185 multiple of order μ of the BPF, $\omega = \mu B \Omega$ reads

$$p_{\mu B}(\mathbf{x}) = \frac{i k_{\mu B} B}{4\pi R} e^{i k_{\mu B} R} \sum_{s=-\infty}^{\infty} e^{i(\mu B - s)(\Phi - \pi/2)} \quad (1)$$

$$\times \left\{ J_{\mu B - s}(\mu B M \sin \Theta) \left[F_s^A \cos \Theta - \frac{(\mu B - s) F_s^T}{\mu B M} \right] + i \sin \Theta F_s^R J'_{\mu B - s}(\mu B M \sin \Theta) \right\},$$

with the notations defined in Fig. 1, where $M = \Omega r / c_0$ is the tangential Mach number of the element and $k_{\mu B} = \mu B \Omega / c_0$ is the acoustic wavenumber. The observer is defined by the spherical coordinates (R, Θ, Φ) in the reference frame $(\mathbf{e}_X, \mathbf{e}_Y, \mathbf{e}_Z)$. In the general case, Eq. (1) is summed over all elements of a discretized blade. For very compact blades, all dimensions of which remain much smaller than the acoustic wavelengths, a single element carrying the instantaneous integrated force is used, located at some averaged radius $r = R_0$.

The complex-valued factors $F_s^{A,T,R}$ are the Fourier coefficients of the axial, tangential and radial components of the aerodynamic force $\mathbf{F}(t)$ on the element, acting as a point dipole. The total Fourier coefficients F_s are related to the algebraic value of the force $F(t)$ by the definition

$$F(t) = \sum_{s=-\infty}^{\infty} F_s e^{-i s \Omega t}, \quad F_s = \frac{\Omega}{2\pi} \int_0^{2\pi/\Omega} F(t) e^{i s \Omega t} dt.$$

In the plane of the rotor disk considered later on for two-dimensional diffraction studies, $\Theta = \pi/2$ and the formula reduces to

$$p_{\mu B}(\mathbf{x}) = \frac{i k_{\mu B} B}{4\pi R} e^{i k_{\mu B} R} \sum_{s=-\infty}^{\infty} e^{i n (\Phi - \pi/2)} \left\{ n F_s^T \frac{J_n(\mu B M)}{\mu B M} + i F_s^R J_n'(\mu B M) \right\},$$

introducing $n = \mu B - s$. Equation (1) states that a tone involves a linear combination of radiation modes. Keeping in mind the time dependence $e^{-i \omega t}$, a single mode at the frequency $\omega = \mu B \Omega$ is defined as a pressure pattern with n angular periods called lobes, the phase of which spins at the angular velocity $\mu B \Omega / n$ associated with a tangential phase Mach number $M_n = \mu B \Omega r / (n c_0)$, if r stands for the radius at which the sources of the mode are considered. In three-dimensional and two-dimensional descriptions, this modal structure combines with spherical and cylindrical wave spreading, respectively, but the angular dependency is the same. In the plane $\Theta = \pi/2$, the symmetric mode associated with the Bessel function J_0 and with the BLH of order $s = \mu B$ can only be excited by the radial force component. The truncation of the infinite sum in Eq. (1) needed for practical predictions is determined by the properties of the Bessel functions: for a fixed value of the argument, the functions rapidly

go to zero for absolute orders exceeding the argument. The blades of a propeller operating in an arbitrary stationary distortion experience a range of BLH orders s . Only a limited interval of them, say between $\mu B - n_{max}$ and $\mu B + n_{max}$ where n_{max} is some integer, possibly give rise to efficient radiation at the frequency $\omega = \mu B \Omega$, because of the weighting by the Bessel function. The range is wider or narrower, depending on either the distortion is concentrated or spread.

For marine propellers, the tangential Mach number $\Omega r/c_0$ is very small, so that for moderate blade numbers and BPF harmonic orders, the argument of the Bessel functions is also small. Furthermore, the tangential phase Mach number is always smaller than 1 for any order $n \neq 0$ (the definition makes no sense for the symmetric mode $n = 0$). Even in non-compact cases, the condition $M_n \ll 1$ corresponds to a negligible radiation efficiency. This makes very poor sound expected in free field from the modal structure of marine propellers, except if the symmetric mode is excited, with $s = \mu B$, for the axial component of blade forces. Therefore, Taylor expansions can be performed to provide a relevant approximation. The limit forms of Bessel functions for small arguments read [14]

$$J_{|n|}(\mu B M) \sim \left(\frac{\mu B M}{2}\right)^{|n|}, \quad J_0(\mu B M) \sim 1,$$

$$J'_{|n|}(\mu B M) \sim \frac{1}{2} \left(\frac{\mu B M}{2}\right)^{|n|}, \quad J'_0(\mu B M) \sim -\frac{\mu B M}{2}.$$

The ratio

$$\frac{J_{|n|}(\mu B M)}{\mu B M} \sim \frac{1}{2^{|n|}} (\mu B M)^{|n|-1}$$

becomes negligible for $|n| \geq 2$, whereas it is 1/2 for $|n| = \pm 1$. This makes the mode orders ± 1 the only significantly contributing ones. These special aspects of vanishing Mach numbers will be re-addressed in section 4.3. Though typical of marine propellers, they are also believed to hold for some small-size, very low-speed fans used in air.

2.2. Source-mode expansion

The sound field of a single mode of order n in Eq. (1) can be exactly reproduced by continuously distributing phased stationary sources of equal am-

220 plitude over the circle of radius r , provided that the phase is tuned to simulate
the angular velocity $\mu B \Omega/n$. The amplitude is defined by the BLH F_s . There-
fore, the phase at any angle ϕ on the circle is defined by the factor $e^{in\phi}$. Such
a distribution is called a source-mode in the present work. Its main interest is
that it provides a representation of the sound field valid at every point in space
225 and not only in the far field, as discussed in references [7, 11, 15]. In particular,
this allows to take into account the near-field terms involved in the scattering
by neighboring surfaces. The stationary point dipole of a source-mode at the
angle ϕ in Fig. 2 has the same instantaneous strength $F(\phi, t)$ as the dipole at
angle $\phi = 0$ but with a time delay $\Delta t = (\mu B - s) \phi/\omega$:

$$\forall \phi \in [0, 2\pi], \quad F(\phi, t) = F(0, t - (\mu B - s)\phi/\omega) . \quad (2)$$

230 This forces the wanted spinning pattern of angular phase speed Ω_s with $n =$
 $\mu B - s$. For the mode of order n associated with the blade-loading harmonic of
order s , $F(\phi, t) = F_s e^{-i\mu B \Omega t}$ with $F_s = A e^{in\phi}$, A being a constant.

3. Cylinder Scattering

3.1. Two-Dimensional Cylinder Green's function

235 An alternative to numerical implementations of the Green's formula, when
solving a problem of acoustics in the presence of solid boundaries, is to consider a
Green's function tailored to the geometry. In the present generic configuration,
the sources are assumed close to a rigid cylinder of circular cross-section. The
exact Green's function, $G(\mathbf{x}, \mathbf{y})$, solution of the homogeneous Helmholtz equa-
240 tion, is determined by adding to the free-field Green's function G_0 a secondary
Green's function G_1 accounting for the scattered field. This scattered part G_1
corresponds to equivalent sources distributed on the surface. Therefore, it is ex-
pressed in terms of cylindrical harmonics. The term G_0 must also be expanded
on the same set of harmonics, in order to formulate the rigid-wall boundary con-
245 dition on the cylinder surface, that must be fulfilled by the complete Green's
function $G = G_0 + G_1$. The procedure is detailed, for instance, in [16]. In polar

coordinates with origin at the center of the cylinder cross-section, and for an observer radius larger than the source radius ($r_x \geq r_y$), the tailored Green's function reads

$$G(\mathbf{x}, \mathbf{y}) = \frac{-i}{4} \left[J_0(kr_y) - \frac{J'_0(ka)}{H_0^{(1)'}(ka)} H_0^{(1)}(kr_y) \right] H_0^{(1)}(kr_x) \quad (3)$$

$$- \frac{i}{4} \sum_{m=1}^{\infty} 2 \cos[m(\theta_y - \theta_x)] \left[J_m(kr_y) - \frac{J'_m(ka)}{H_m^{(1)'}(ka)} H_m^{(1)}(kr_y) \right] H_m^{(1)}(kr_x)$$

if a stands for the cylinder radius. x and y as indices stand for the observer and source coordinates, respectively. In the opposite configuration ($r_x < r_y$), the products $J_m(kr_y) H_m^{(1)}(kr_x)$ corresponding to the first terms in the squared brackets must be replaced by $H_m^{(1)}(kr_y) J_m(kr_x)$. In fact, these terms stand for the free-field Green's function $G_0(\mathbf{x}, \mathbf{y})$, expressed in the coordinate system of the cylinder. The other terms involving ratios of derivatives account for the scattering by the cylinder. All exact calculations performed in the present work, for arbitrary dipole source-modes, are performed by making the scalar product of the local dipole strength by the first gradient of the Green's function G with respect to the source coordinates. This provides the value of the radiated sound field at any point of space as

$$p = \mathbf{F}_s \cdot \nabla(G_0 + G_1),$$

250 with $\mathbf{F}_s = F_s \mathbf{n}_\phi$, where \mathbf{n}_ϕ is the unit vector along the dipole axis of angular location ϕ along the source-mode circle and $F_s = F e^{i n \phi}$ is the dipole strength. The derivations of $\nabla(G_0 + G_1)$ are not detailed here for conciseness. They are similar to those provided by Gloerfelt *et al.* [17], who investigated the radiation of quadrupoles in the presence of a cylinder. The scattering is calculated for
 255 each point dipole of a source-mode and the total field is obtained through an integral over the circle. Practically, this integral is discretized as a finite sum for implementation. A similar approach has been detailed by Roger & Moreau [11] in the investigation of the scattering of fan/propeller noise in the air by the edge of a rigid half-plane.

The asymptotic analysis leading to the compact regime of the Green's function is mainly focused on the part G_1 , responsible for amplification. However, special cases also require a comparison with the direct field. Let's note:

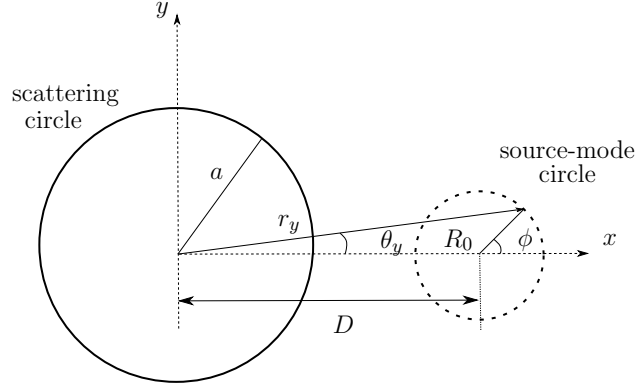


Figure 2: Coordinates of a source mode close to a scattering cylinder for the asymptotic calculations. Note that $D = L + a$ (see Fig. 1).

$$\frac{J'_0(ka)}{H_0^{(1)'}(ka)} = \frac{J_1(ka)}{H_1^{(1)}(ka)} = \Phi_0, \quad \frac{J'_m(ka)}{H_m^{(1)'}(ka)} = \frac{J_{m-1}(ka) - J_{m+1}(ka)}{H_{m-1}^{(1)}(ka) - H_{m+1}^{(1)}(ka)} = \Phi_m.$$

Consider an observer in the acoustic far field and distributed sources over a circle remaining close to the scattering cylinder, the latter being acoustically compact, so that

$$kr_x \gg 1, kr_y \ll 1, ka \ll 1,$$

In the present application, source points are distributed over a circle of radius R_0 , the center of which is at some small distance D from the center of the cylinder, in such a way that also $kD \ll 1$ and $kR_0 \ll 1$ (circular arrays of dots in Figs. 1 and 2). This refers to the so-called compact Green's function framework. In this case, asymptotic expansions can be used to derive a simplified form of

the Green's function. For large arguments [14],

$$H_m^{(1)}(kr_x) \sim \sqrt{\frac{2}{\pi kr_x}} e^{i[kr_x - m\pi/2 - \pi/4]},$$

whereas for small arguments

$$H_m^{(1)}(kr_y) \sim \frac{-i}{\pi} \Gamma(m) \left(\frac{2}{kr_y}\right)^m \quad \text{and} \quad J_m(kr_y) \sim \frac{1}{\Gamma(m+1)} \left(\frac{kr_y}{2}\right)^m, \quad m \geq 1$$

$$H_0^{(1)}(kr_y) \sim \frac{2i}{\pi} \ln\left(\frac{kr_y}{2}\right) \quad \text{and} \quad J_0(kr_y) \sim 1 - \left(\frac{kr_y}{2}\right)^2.$$

Introducing these developments in the definition of the factor Φ_m for small values of ka yields

$$\Phi_0 \sim i\pi \left(\frac{ka}{2}\right)^2, \quad \Phi_m \sim \frac{-i\pi}{\Gamma(m)\Gamma(m+1)} \left(\frac{ka}{2}\right)^{2m}.$$

For consistency, ka and kr_y must be assumed as small quantities of the same order of magnitude.

Once introducing the asymptotic developments in the expression of the exact Green's function, the first step to the limit form of the Green's function G_1 is obtained as

$$G_{1as}(\mathbf{x}, \mathbf{y}) \sim \frac{-i}{4} f(r_x) \left(\frac{ka}{2}\right)^2 2 \ln\left(\frac{kr_y}{2}\right) - \frac{i}{4} f(r_x) \sum_{m=1}^{\infty} 2 \cos[m(\theta_y - \theta_x)] \frac{e^{-im\pi/2}}{\Gamma(m+1)} \left(\frac{ka}{2}\right)^m \left(\frac{a}{r_y}\right)^m,$$

with

$$f(r_x) = \sqrt{\frac{2}{\pi kr_x}} e^{i[kr_x - \pi/4]}.$$

Next assuming that a/r_y is of order 1 leads to retain only the leading term $m = 1$. Finally

$$G_{1as}(\mathbf{x}, \mathbf{y}) \sim \frac{-i}{2} f(r_x) \left(\frac{ka}{2}\right)^2 \left[\ln\left(\frac{kr_y}{2}\right) - i \cos(\theta_y - \theta_x) \left(\frac{2}{kr_y}\right) \right].$$

Space derivatives of the Green's function with respect to source coordinates are required when calculating the sound from dipoles. In the radial derivative the logarithm can be neglected as negligible compared to the other term. The first gradient components are finally obtained as

$$\frac{\partial G_{1as}}{\partial r_y} = f(r_x) \left(\frac{ka}{2}\right)^2 \frac{\cos(\theta_y - \theta_x)}{kr_y^2}, \quad \frac{1}{r_y} \frac{\partial G_{1as}}{\partial \theta_y} = f(r_x) \left(\frac{ka}{2}\right)^2 \frac{\sin(\theta_y - \theta_x)}{kr_y^2}. \quad (4)$$

270 It is worth noting that the compact Green's function and its derivatives no longer involve indices $m > 1$.

3.3. Asymptotic Free-Field Green's Function

Subsequent needs also require the derivatives of the free-field Green's function G_0 . In the compact regime, the latter reads

$$G_{0as}(\mathbf{x}, \mathbf{y}) \sim \frac{-i}{4} f(r_x) \left[1 - \left(\frac{kr_y}{2}\right)^2 - 2i \cos[(\theta_y - \theta_x)] \left(\frac{kr_y}{2}\right) \right].$$

For the radial derivative, the term $(kr_y/2)^2$ can be discarded as negligible compared to the other terms. Finally, the approximations are obtained as:

$$\frac{\partial G_{0as}}{\partial r_y} = -\frac{k}{4} f(r_x) \cos(\theta_y - \theta_x), \quad \frac{1}{r_y} \frac{\partial G_{0as}}{\partial \theta_y} = \frac{k}{4} f(r_x) \sin(\theta_y - \theta_x), \quad (5)$$

with

$$f(r_x) = \sqrt{\frac{2}{\pi kr_x}} e^{i[kr_x - \pi/4]}.$$

275 4. Radiation of Compact Spinning Source-Modes

The expressions of the previous section are now used to calculate the far-field sound pressure radiated by a compact source mode of arbitrary order. Derivations are first detailed for purely tangential dipoles; the case of radial dipoles is then summarized for completeness.

280 4.1. Point-Dipole Formula

In the present section, for any point dipole of a source mode, the dipole axis is assumed tangent to the source-mode circle. This restriction would be exact for a purely axial-flow propeller, with unswept blades. With the notations in Fig. 2, the point dipole of angular coordinate ϕ along the source circle and of

unit strength has the radial and angular components in the reference frame of the scattering cylinder

$$F_r = -\frac{D}{r_y} \sin \phi e^{i n \phi}, \quad F_\theta = \frac{R_0 + D \cos \phi}{r_y} e^{i n \phi},$$

for the spinning mode of order n , with

$$r_y^2 = D^2 + R_0^2 + 2 D R_0 \cos \phi, \quad \tan \theta_y = \frac{\sin \phi}{\cos \phi + D/R_0}.$$

The scattered sound pressure of the point dipole in the asymptotic regime reads

$$p_1(r_x, \theta_x) = F_r \frac{\partial G_{1as}}{\partial r_y} + \frac{F_\theta}{r_y} \frac{\partial G_{1as}}{\partial \theta_y},$$

After rearranging terms:

$$\frac{k p_{1as}(r_x, \theta_x)}{f(r_x) (ka/2)^2} = \cos \theta_x (R_0^2 - D^2) \frac{\sin \phi e^{i n \phi}}{r_y^4} - \sin \theta_x \left[(R_0^2 + D^2) \frac{\cos \phi e^{i n \phi}}{r_y^4} + 2 R_0 D \frac{e^{i n \phi}}{r_y^4} \right] \quad (6)$$

According to the same principles as for the diffracted field, the direct sound pressure radiated by the point dipole in the asymptotic regime is :

$$p_{0as}(r_x, \theta_x) = F_r \frac{\partial G_{0as}}{\partial r_y} + \frac{F_\theta}{r_y} \frac{\partial G_{0as}}{\partial \theta_y}$$

After developing terms, it is expressed as

$$\begin{aligned} \frac{p_{0as}(r_x, \theta_x)}{f(r_x) (k/4)} &= \cos \theta_x \left[(R_0^2 + D^2) \frac{\sin \phi e^{i n \phi}}{r_y^2} + 2 R_0 D \frac{\cos \phi \sin \phi e^{i n \phi}}{r_y^2} \right] \quad (7) \\ &- \sin \theta_x \left[(R_0^2 + D^2) \frac{\cos \phi e^{i n \phi}}{r_y^2} + R_0 D \frac{e^{i n \phi}}{r_y^2} + R_0 D \frac{\cos 2 \phi e^{i n \phi}}{r_y^2} \right] \end{aligned}$$

The total sound of the source mode is obtained by performing the integration on the circle for equation (6) and equation (7), from $\phi = -\pi$ to $\phi = +\pi$. The resulting closed-form expressions are developed in the next section.

285

4.2. Case of Higher-Order Modes

From the previous section, three integrals involving the quantities $\cos \phi$, $\sin \phi$ and $e^{i n \phi}$ and the factor r_y^4 in the denominator must be calculated. These

integrals result in closed-form expressions, making use of tables by Gradshteyn & Ryzhik [18] (pages 391-394) and noting that the odd-function parts can be discarded from the integrands. For $n \geq 2$ the individual integrals are found as

$$\begin{aligned} \int_{-\pi}^{\pi} \frac{\cos \phi e^{i n \phi}}{r_y^4} d\phi &= \frac{\pi}{D^4} \frac{(-R_0/D)^{n-1}}{[1 - (R_0/D)^2]^3} \left\{ 4 \left(\frac{R_0}{D} \right)^2 + n \left[1 - \left(\frac{R_0}{D} \right)^4 \right] \right\}, \\ \int_{-\pi}^{\pi} \frac{\sin \phi e^{i n \phi}}{r_y^4} d\phi &= \frac{n i \pi}{D^4} \frac{(-R_0/D)^{n-1}}{[1 - (R_0/D)^2]^3}, \\ \int_{-\pi}^{\pi} \frac{e^{i n \phi}}{r_y^4} d\phi &= \frac{2\pi}{D^4} \frac{(-R_0/D)^n}{[1 - (R_0/D)^2]^3} \left[n + 1 - (n-1) \left(\frac{R_0}{D} \right)^2 \right]. \end{aligned}$$

Regrouping all terms in the developed expression of the acoustic pressure leads to the final result

$$p_{1as}(r_x, \theta_x) \sim -i \frac{\pi k}{4} n \left(\frac{a}{D} \right)^2 \left(\frac{-R_0}{D} \right)^{n-1} e^{-i \theta_x} \sqrt{\frac{2}{\pi k r_x}} e^{i(k r_x - \pi/4)}. \quad (8)$$

The most important feature is that, whatever the positive order n of the source mode is, the asymptotic scattering by the compact Green's function of the cylinder generates the mode $m = -1$, thus with a single lobe and spinning in the opposite direction. The factor $n(-R_0/D)^{n-1}$ is involved in the amplification of the direct mode. Of course, the mode $m = +1$ is similarly produced for any negative order n .

In order to assess the asymptotic formulation, the decrease of the scattered sound with observer distance r_x is plotted in Fig. 3, for a source-mode located at the dimensionless distance $kL = 0.1$ from the cylinder edge and various mode orders $n > 1$. The global compactness is ensured for all configurations. The sound pressure level is averaged over a full circle $\theta_x \in [0, 2\pi]$. The dashed and solid lines stand for the exact analytical solution, Eq. (3), and for the asymptotic formulation, Eq. (8), respectively. The results are twofold. Firstly, both solutions nearly coincide beyond $kr_x = 3$, where the far-field decay $1/\sqrt{r_x}$ is reached. Secondly, the amplitude of the scattered pressure decreases as the mode order increases, for the same dipole source strength, as expected from the factor $n(R_0/D)^{n-1}$. More precisely, overall level differences of about 8.6 dB, 9.6 dB, 10.2 dB are predicted from the term $20 \log_{10}[n(R_0/D)^{n-1}]$ between the

scattered sounds of the pairs of mode orders $(n = 2, n = 3)$, $(n = 3, n = 4)$ and $(n = 4, n = 5)$, respectively. The same test for special cases is also reported in Fig. 4 in the next section.

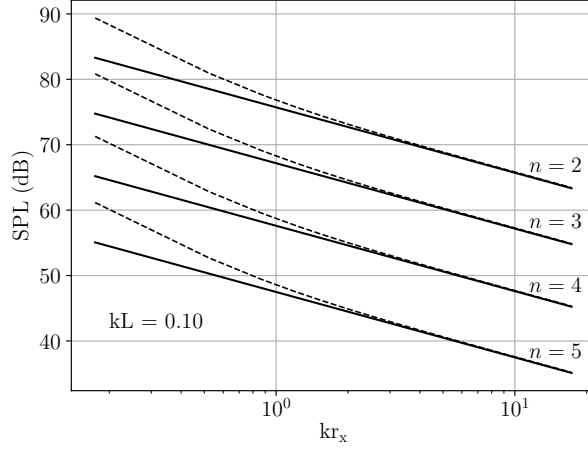


Figure 3: Sound pressure level decrease of a source-mode located nearby a rigid cylinder for higher-order modes, $n > 1$. $kR_0 = 0.034$, $R_0/D = 0.25$, $kL = 0.10$. Exact (---) and asymptotic (—) solutions.

The amplification itself is better recognized if now the free field of the same arbitrary mode $n > 1$ is calculated, also referring to the same asymptotic developments, from Eqs. (7). The following integrals are involved:

$$\begin{aligned} \int_{-\pi}^{\pi} \frac{\cos \phi e^{in\phi}}{r_y^2} d\phi &= \frac{\pi (-R_0/D)^{n-1}}{D^2 [1 - (R_0/D)^2]} [1 + (R_0/D)^2], \\ \int_{-\pi}^{\pi} \frac{\cos 2\phi e^{in\phi}}{r_y^2} d\phi &= \frac{\pi (-R_0/D)^{n-2}}{D^2 [1 - (R_0/D)^2]} [1 + (R_0/D)^4], \\ \int_{-\pi}^{\pi} \frac{\sin \phi e^{in\phi}}{r_y^2} d\phi &= \frac{i\pi}{D^2} (-R_0/D)^{n-1}, \\ \int_{-\pi}^{\pi} \frac{\sin \phi \cos \phi e^{in\phi}}{r_y^2} d\phi &= \frac{i\pi}{2D^2} (-R_0/D)^{n-2} [1 + (R_0/D)^2], \\ \int_{-\pi}^{\pi} \frac{e^{in\phi}}{r_y^2} d\phi &= \frac{2\pi}{D^2} \frac{(-R_0/D)^n}{[1 - (R_0/D)^2]}. \end{aligned}$$

310 Reproducing similar derivations as for the function G_{1as} with the same source mode now leads to an exactly zero pressure field. This means that, at the

leading order of the asymptotic regime, the free field contribution is negligible compared to the scattered field, confirming the amplification mechanism.

4.3. Special Cases

Equation (8) of the previous section holds for $n \geq 2$. Special developments are required for the mode $n = 1$, leading to consider the new integrals

$$\begin{aligned} \int_{-\pi}^{\pi} \frac{\sin \phi e^{i\phi}}{r_y^4} d\phi &= \frac{i\pi}{D^4 [1 - (R_0/D)^2]}, \\ \int_{-\pi}^{\pi} \frac{\cos \phi e^{i\phi}}{r_y^4} d\phi &= \frac{\pi}{D^4 [1 - (R_0/D)^2]^3} \left[1 + 4 \left(\frac{R_0}{D} \right)^2 - \left(\frac{R_0}{D} \right)^4 \right], \\ \int_{-\pi}^{\pi} \frac{e^{i\phi}}{r_y^4} d\phi &= \frac{4\pi}{D^4} \frac{(-R_0/D)}{[1 - (R_0/D)^2]^3}. \end{aligned}$$

315 When this is applied to derive the radiation of the source-mode $n = 1$, the expression follows as

$$p_{1as}(r_x, \theta_x) \sim -i \frac{\pi k}{4} \left(\frac{a}{D} \right)^2 e^{-i\theta_x} \sqrt{\frac{2}{\pi k r_x}} e^{i(kr_x - \pi/4)}. \quad (9)$$

Again the mode -1 is found in the scattered field (the expression is in fact Eq. (8) with $n = 1$) but now the direct field derived following the same principles implies the integrals

$$\begin{aligned} \int_{-\pi}^{\pi} \frac{\cos \phi e^{i\phi}}{r_y^2} d\phi &= \pi \frac{1 + (R_0/D)^2}{D^2 [1 - (R_0/D)^2]}, \\ \int_{-\pi}^{\pi} \frac{\cos 2\phi e^{i\phi}}{r_y^2} d\phi &= \pi \frac{1 + (R_0/D)^2}{D^2 [1 - (R_0/D)^2]} (-R_0/D), \\ \int_{-\pi}^{\pi} \frac{\sin \phi e^{i\phi}}{r_y^2} d\phi &= \frac{i\pi}{D^2}, \\ \int_{-\pi}^{\pi} \frac{\sin \phi \cos \phi e^{i\phi}}{r_y^2} d\phi &= \frac{i\pi}{2D^2} (-R_0/D), \\ \int_{-\pi}^{\pi} \frac{e^{i\phi}}{r_y^2} d\phi &= 2\pi \frac{(-R_0/D)}{D^2 [1 - (R_0/D)^2]}. \end{aligned}$$

320 It is found as

$$p_{0as}(r_x, \theta_x) \sim i \frac{\pi k}{4} e^{i\theta_x} \sqrt{\frac{2}{\pi k r_x}} e^{i(kr_x - \pi/4)}, \quad (10)$$

which corresponds to significant radiation, of similar efficiency as for the scattered field. The asymptotic scattering causes no amplification in this case, unlike for higher-order modes, since the factor a/D is smaller than 1. Equation (9) is a minor perturbation of the direct field, Eq. (10). This is confirmed by the test reported in Fig. 4. The exact and asymptotic solutions of the direct and scattered parts for the special case $n = 1$, averaged over all observation angles, are plotted as a function of the observer distance. The level difference of about 5 dB between the scattered and direct sounds is well predicted by the far-field estimate $20 \log_{10}(a/D)^2$ from Eqs. (9) and (10). Then, as seen previously for higher-order modes, both solutions perfectly match above $kr_x = 3$, which defines the validity limit of the asymptotic formulation.

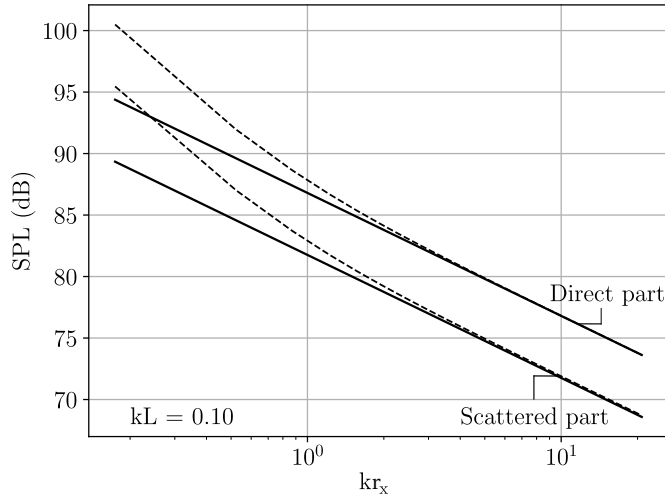


Figure 4: Sound pressure level decrease of a source-mode located nearby a rigid cylinder for the mode $n = 1$. $kR_0 = 0.034$, $R_0/D = 0.25$, $kL = 0.10$. Exact (---) and compact approximations (—) of the direct and scattered parts of the Green's function.

The special behavior of the mode $n = 1$ can be explained by simple physical considerations. For this mode, two diametrically opposite dipoles are in phase

opposition, which means that they point in the same direction. They double
335 each other in amplitude because the diameter is acoustically compact. The total
source mode is equivalent to a spinning point dipole.

A similar discussion can be made about the symmetric source mode $n = 0$,
for which diametrically opposite dipoles now point in opposite directions because
they are in phase. They cancel each other, so that the expected radiation of
340 the mode is zero in the compact limit. This can be verified easily by repeating
the previous analysis in the case $n = 0$: both the asymptotic free field and
the asymptotic scattered field are zero. Important consequences follow when
transposing these results to installed marine propellers. The symmetric mode is
known to be only generated by interaction of the propeller with the distortion
345 harmonic of order $s = \mu B$ at any BPF order μ . It should not be a major
issue, unlike in the case of aircraft propellers, because it cannot experience
amplification by hull scattering. In contrast, the analysis reveals that the modes
 $n = \pm 1$ are expectedly the most efficient ones, both in free field and in the
presence of a hull. These modes are likely to be excited at the lowest frequencies
350 for installed propellers with quite small blade numbers.

It is worth noting that the selective amplification associated with asymp-
totic scattering leads to the possible need to reconsider the assumption of a
single equivalent dipole on each blade, even if the blade is compact. Indeed,
source points close to blade tip and close to hub experience different amounts of
355 scattering. Such a 'de-compacification' is beyond the scope of the present study.

4.4. Case of a Radial Force

The complementary case of a radial force component in the sense of the
propeller or of the modal circle is considered in this section for completeness.
Indeed, such a dipole is part of the loading noise of a twisted swept blade,
even if not dominant in an axial-flow architecture. Furthermore, formulations
of the thickness noise detailed, for instance, in references [1, 3], involve a radial
dipole associated with the centripetal acceleration. In the reference frame of
the cylinder in Fig. 2, the radial and tangential components of a point dipole of

angle ϕ become

$$F_r = \frac{R_0 + D \cos \phi}{r_y} e^{i n \phi}, \quad F_\theta = \frac{D}{r_y} \sin \phi e^{i n \phi},$$

and the far-field scattered pressure is deduced as

$$\begin{aligned} \frac{k p_{1as}(r_x, \theta_x)}{f(r_x) (ka/2)^2} &\simeq \sin \theta_x (R_0^2 - D^2) \frac{\sin \phi e^{i n \phi}}{r_y^4} \\ &+ \cos \theta_x \left[(R_0^2 + D^2) \frac{\cos \phi e^{i n \phi}}{r_y^4} + 2 R_0 D \frac{e^{i n \phi}}{r_y^4} \right]. \end{aligned}$$

The derivations can be repeated, using the same integrals as for the tangential dipoles. They lead to the very similar result for the case of higher modes, $n \geq 2$:

$$\begin{aligned} p_{1as}(r_x, \theta_x) &\sim \frac{\pi k}{4} n \left(\frac{a}{D}\right)^2 \left(\frac{-R_0}{D}\right)^{n-1} e^{-i \theta_x} \sqrt{\frac{2}{\pi k r_x}} e^{i(kr_x - \pi/4)}, \quad (11) \\ p_{0as}(r_x, \theta_x) &\sim 0, \end{aligned}$$

which differs from Eq. (8) only by a phase quadrature. This difference is also
 360 found in the special case $n = 1$, where the scattered and the direct field read:

$$p_{1as}(r_x, \theta_x) \sim -i \frac{\pi k}{4} \left(\frac{a}{D}\right)^2 e^{-i \theta_x} \sqrt{\frac{2}{\pi k r_x}} e^{i[kr_x + \pi/2 - \pi/4]}, \quad (12)$$

$$p_{0as}(r_x, \theta_x) \sim i \frac{\pi k}{4} e^{i \theta_x} \sqrt{\frac{2}{\pi k r_x}} e^{i[kr_x + \pi/2 - \pi/4]}. \quad (13)$$

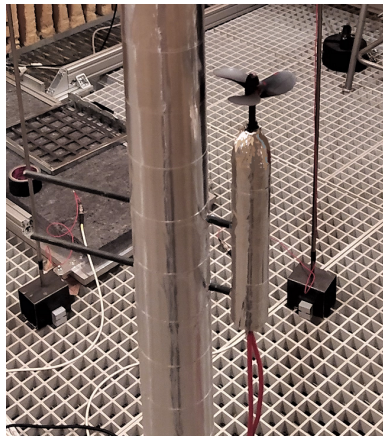
For the mode $n = 1$, the result is due to the fact that diametrically opposite
 radial dipoles are again aligned and double each other in the compact limit. The
 resulting equivalent point dipole is just spinning with an angular phase shift of
 365 $\pi/2$ with respect to the point dipole of the tangential-force mode because they
 are perpendicular to each other.

5. Small-Scale In-Air Experiment

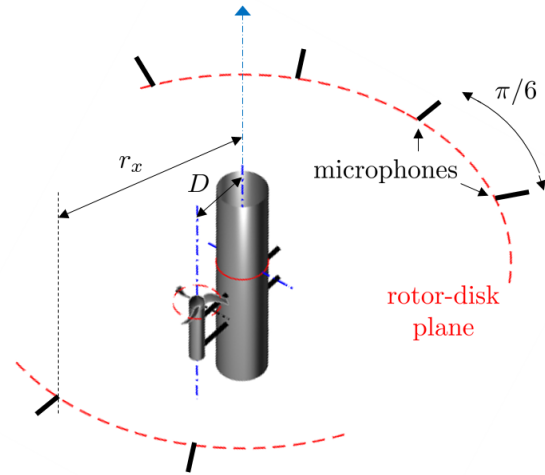
5.1. Setup

370 For validation purposes, a small-scale experiment has been performed, aimed at confirming the asymptotic amplification associated with the compact Green's function. The experiment is made in air for simplicity. A three-bladed propeller of 63 mm blade-tip diameter is mounted at one end of a cylindrical hub of diameter 27 mm and length 170 mm, as shown in Fig. 5-a. It is powered by a Maxon DC-motor (type 2 322.980-52) of 21 mm diameter inserted in the hub at two regimes, referred to as the low speed (11800 rpm) and high speed (14800 rpm), corresponding to blade-tip Mach numbers of about 0.1 and 0.14, respectively. The scattering cylinder has a diameter of 60 mm and a length of 1 m. The propeller plane is at mid-length of the cylinder. The hub is placed parallel to the cylinder at varying distance D , by means of diametrically sliding rods of 5 mm diameter. The latter are believed to have a negligible effect on the relative variations of the sound resulting from changes in D .

380



(a)



(b)

Figure 5: (a): picture of the small-scale propeller-cylinder mockup installed in the anechoic room of Ecole Centrale de Lyon. (b): sketch of the setup for measurements in the propeller-disk plane (featured by red circles).

Table 1: 20 Hz-bandwidth peak levels and Helmholtz numbers at the BPF as a function of D (mm), for both tested rotational speeds.

	$D = 65$	$D = 70$	$D = 85$	$D = 95$	$D = 168$
low speed (dB)	48.3	49.1	42.55	38.2	35.3
$(ka = 0.35) kD$	0.71	0.76	0.92	1.04	1.83
$k(D - [R_0 + a])$	0.030	0.084	0.25	0.35	1.15
high speed (dB)	55.1	52.7	48	46	45.7
$(ka = 0.44) kD$	0.88	0.96	1.16	1.30	2.30
$k(D - [R_0 + a])$	0.037	0.11	0.31	0.45	1.45

The mock-up is installed vertically in an anechoic room, according to the sketch in Fig. 5-b. Twelve 1/4" microphones (GRAS type 46BE) are placed at
385 azimuths $j 2\pi/12$ ($0 \leq j \leq 11$) in the plane of the propeller disk, at a measuring distance r_x of 1.2 m from the cylinder axis. The condition of acoustic far-field at the first BPF is already ensured at this distance. The origin of coordinates is taken on the cylinder axis because the asymptotic scattering involves secondary sources distributed on the cylinder, which are much more efficient than the
390 primary sources on the blades. The microphones are inserted horizontally into L-shaped vertical supports of 8 mm diameter, pointing toward the cylinder axis. This instrumentation is believed to cause negligible spurious scattering.

The two rotational speeds correspond to BPF of 590 Hz and 740 Hz. They are tested for various values of the axis-to-axis distance D . The shortest distance
395 of 65 mm only leaves a minimum gap of about 2 mm between the blade tip passages and the cylinder. The largest one is of 168 mm. The corresponding dimensionless parameters are summarized in Table 1.

The experiment is mainly aimed at highlighting the characteristic amplification, with the generation of the mode -1. The precise blade design and a
400 complete inspection of the propeller aerodynamics are beyond the scope of the study. This would have typically required advanced optical flow-measurement techniques at the very small scale of the experiment, in order to avoid intrusive-

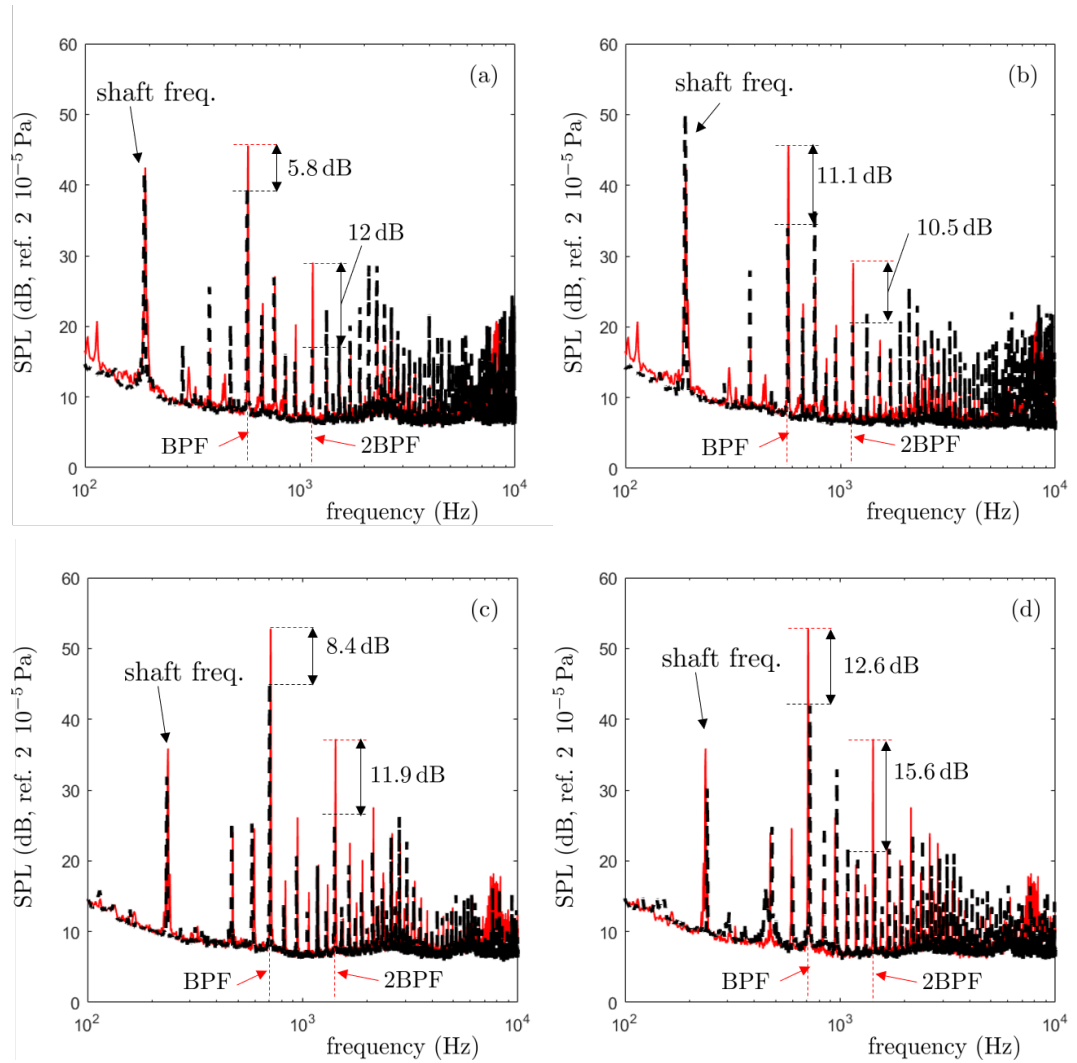


Figure 6: Compared sound-pressure spectra for axis-to-axis distances $D = 65$ mm (red) and $D = 85$ mm (black) in the left column ((a) & (c)), and for $D = 65$ mm (red) and $D = 140$ mm (black) in the right column ((b) & (d)). (a) & (b): low rotational speed; (c) & (d): high rotational speed.

ness.

5.2. Sound-Pressure Spectra

405 Typical spectra (PSD, power spectral densities) of the measured sound pressure, averaged on all microphones of the array, are shown in Fig. 6. The averaging provides a relevant global characterization of the radiated sound field, as long as the angular variations along the array remain small. This is the case for the direct field at the first two BPF tones, as well as for the total field in the
410 presence of the cylinder in the compact configuration of minimum separation D , at least for the BPF, as shown in Fig. 7. The significant angular variations for the installed configuration at twice the BPF, in Fig. 7-b, are not believed to question the final conclusions. The resolution in Fig. 6 is of 1 Hz and the acquisition time of 30 s ensures convergence. Two spectra are superimposed
415 on each plot, one for the shortest value of D (65 mm) and the other one for $D = 85$ mm (in Fig. 6-a & c) and $D = 140$ mm (in Fig. 6-b & d). This enables to identify the amplification of the first two BPF tones, marked by the double arrows. The associated values of the tonal-noise level differences are also reported on the plots, after integration of the PSD in 20-Hz bandwidths
420 centered on the peak values. This eliminates the possible time variations of the rotational speed. These differences are slightly larger than the peak-to-peak differences illustrated by the double arrows. A significant increase of the third tone can also be noticed at the higher rotational speed (Fig. 6-c & d). The key result is that the levels at the first two BPF tones dramatically increase as
425 the propeller approaches the cylinder, to the shortest distance. The increase at the BPF is of 11.1 dB for the low speed and of about 12.6 dB for the high speed, going from $D = 140$ mm to $D = 65$ mm. It is worth noting that the sound spectrum also includes other tones not directly related to propeller noise. The shaft rotational frequency and some of its harmonics are attributed
430 to mechanical imbalance. The multiple tonal, haystack-like signature at higher frequencies, beyond 2BPF, is probably produced by the electric motor. The specificity of the BPF tones is their modal structure, expressed by Eq. (1) and

investigated in the next section. The amplification pointed out in the present work is *a priori* a typical consequence of this structure. Therefore only the BPF tones are addressed.

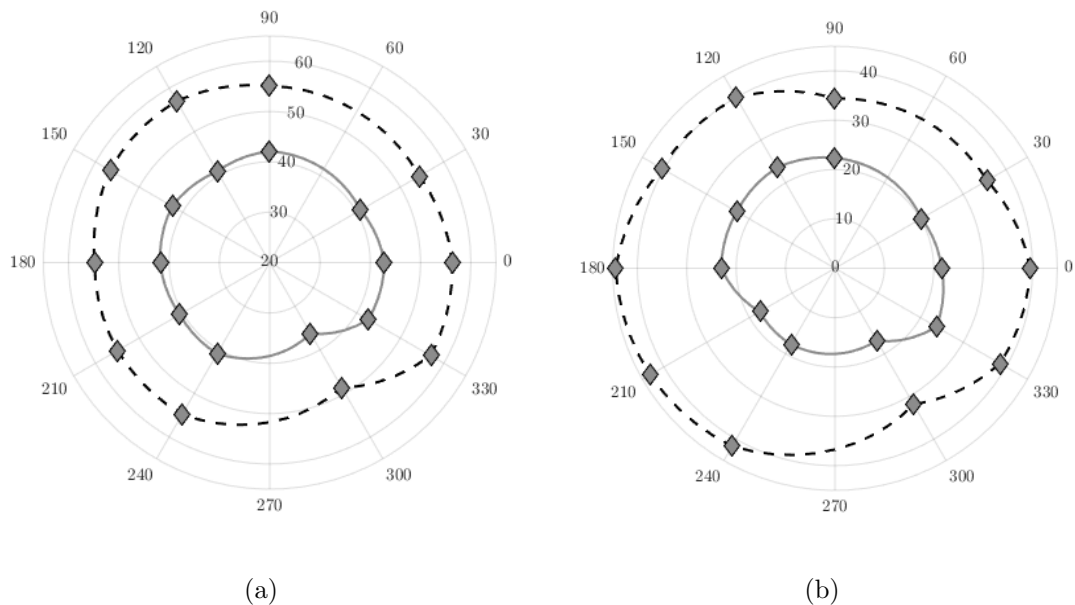


Figure 7: Directivity diagrams in the (x,y) plane at the BPF (a) and twice the BPF (b), with linear interpolation between measuring positions (symbols \diamond). (—): Free-field measurements for the centered propeller ($D = 0$). (- - -): installed propeller at $D = 65$ mm. Different dB scales in the two sub-plots.

Additional results discussed for completing the argumentation are shown in Fig. 8. Figure 8-a compares the averaged sound spectrum measured for the minimum distance $D = 65$ mm to averaged free-field spectra measured after removing the cylinder. Two positions of the propeller axis, namely at the center of the microphone array and shifted by $D = 168$ mm, are considered, providing nearly the same BPF tone levels, highlighted by small ellipses. The figure illustrates the maximum amount of scattering by the cylinder.

The increase of propeller tonal noise associated with the presence of the cylinder could result from any of two mechanisms. The first one is the amplification inherent to the asymptotic regime of the Green's function, expected from

the theoretical analysis of section 4. The second one is the possible generation of stronger blade-loading harmonics, as an effect of higher stationary flow distortions. Indeed, the flow the propeller would have in free field, especially around the blade tips, can be modified as the blades get close to the cylinder because
450 of some flow blockage. Investigating such aerodynamic changes would require a specific instrumentation, well beyond the scope of the present study. Therefore, simple indirect considerations only based on far-field acoustic measurements are used to state about that point. The first step is a complementary measurement performed after replacing the cylinder by a large rigid plate mounted vertically
455 and approached at the same distance to the blade tips as in the configuration $D = 65$ mm. The plate is 1.2 m high and 0.6 m wide, the propeller being placed close to its center point. It is believed to have aerodynamic effects similar to those of the cylinder at the scale of the blade tip-flow details, which makes qualitatively the same order of magnitude of the blade-loading harmonics expected, if any. However, unlike the cylinder, the plate causes pure reflection
460 of the direct sound from the propeller. For plate dimensions much larger than the wavelength, the image principle would hold. Applying this principle to a simple point source at vanishing distance, a doubling of the measured sound-pressure amplitude, thus a maximum sound increase of 6 dB, would be found
465 for measuring locations facing the plate, instead of the amplification. The case of the propeller is less simple. The result of the test is reported in Fig. 8-b. But because the averaging procedure leading to Fig. 6 would make no sense in the presence of the plate, the spectra have been averaged only on the two microphones located around $\pm 15^\circ$ from the direction normal to the plate. The
470 BPF tone levels in free-field condition and with the plate installed, with 20-Hz bandwidth integration, are 42.5 dB and 46.3 dB, respectively, whereas the level reaches 58.6 dB with the cylinder in the configuration $D = 65$ mm. The increase of $46.3 - 42.5 = 3.8$ dB remains compatible with a sound-reflection effect, and suggests that the regeneration of blade-loading harmonics is either moderate or
475 negligible. The much higher sound increase of $58.6 - 42.5 = 16.1$ dB is logically attributable to the aforementioned amplification mechanism.

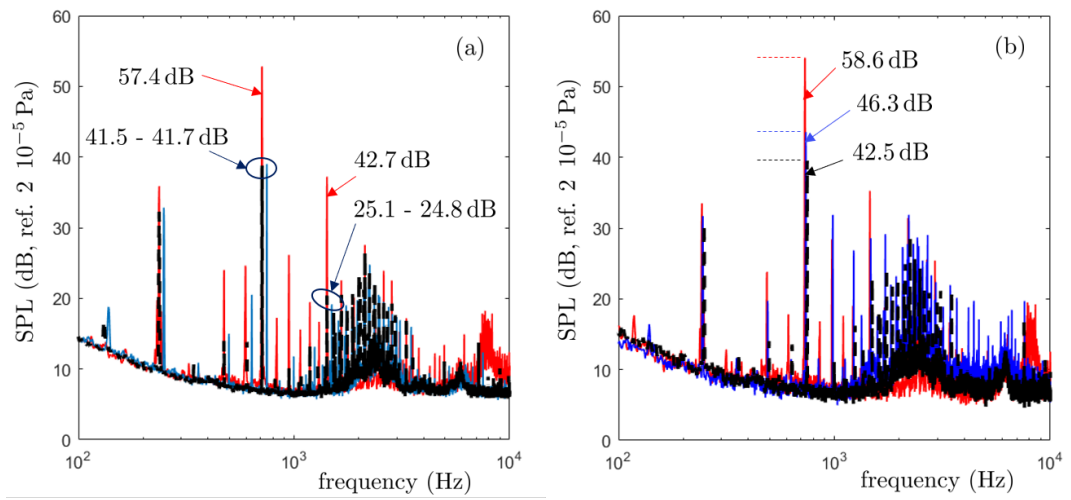


Figure 8: (a): free-field sound spectra of the propeller, at the center of the microphone array (blue) and shifted by $D = 168$ mm (black), compared to the spectrum measured with the cylinder installed at $D = 65$ mm (red); average over the complete array. (b): sound-pressure spectra of the propeller, in free field (black), close to a reflecting plate (red, blade-tip to wall gap 2 mm) and close to the cylinder (blue, $D = 65$ mm); two-microphone average. High speed case, BPF = 740 Hz.

Approaching a side-plate to a rotor disk has also been found to increase the tonal noise in previous studies, because of both the reflection effect and the aerodynamic interaction. The latter is presumably more noticeable at high
480 speeds, when an axial flow and the associated boundary layer develop over the plate. Whatmore & Lawson reported various tonal noise increases of up to 8-10 dB in such a configuration, for a typical tip Mach number around 0.22 and a blade-tip radius of 33 cm [19]. Such a strong effect is not expected in the present study because of the lower Mach numbers of 0.1 and 0.14, at the
485 two tested speeds. Yet the 8-10 dB increase can be considered as a maximum expectable effect, which remains much lower than the actual increase observed in the presence of the cylinder.

Apart from the variations in tone levels, all spectra in Figs. 6 and 8 exhibit similar broadband noise levels below 1.7 kHz, and small differences at higher
490 frequencies. The latter are not interpreted in the present study. Indeed, the broadband noise is much lower than the tonal noise of interest, and always limited by a threshold of about 7 dB corresponding to the electronic background noise.

The main outcome of this section is that reducing the gap between the blade
495 tips and a reflecting plate causes tonal noise increases which remain much lower than those with the same gap and the cylinder. It is concluded that the large noise increase observed with the cylinder is rather a sound-scattering effect than an aerodynamic effect. This is confirmed in the next section by performing an expansion of the sound field in the rotor-disk plane into azimuthal modes of
500 radiation.

5.3. Modal Content of the Radiated Field

Free-field formulations of tonal propeller noise, reminded in section 2.1, indicate that the sound field of any harmonic of the BPF is a sum of spinning modes of radiation, as viewed from the propeller reference frame ($\mathbf{e}_X, \mathbf{e}_Y, \mathbf{e}_Z$)
505 (Fig. 1). The scattering of this direct field by the cylinder generates a secondary field also made of modes, as viewed from the cylinder reference frame.

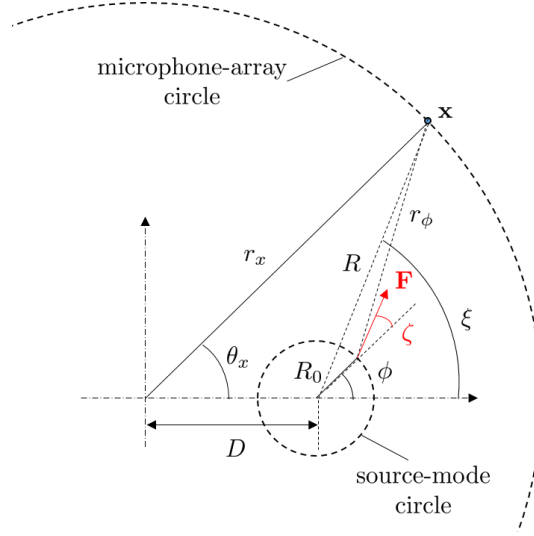


Figure 9: Coordinates of a point on the circle of the microphone array and relative to the off-axis source circle.

In the installed configuration, the propeller axis is displaced by an amount D off the origin of the center of the microphone array. This makes the modal signature of the direct sound radiated by the propeller hard to recognize in the modal expansion of the total sound field. Indeed, the latter is performed taking the cylinder axis as origin, whereas the former makes sense with origin on the propeller axis. Except for vanishing ratio D/λ , a direct propeller mode of order n is interpreted by the array processing as a range of modes, in the reference frame of the cylinder. This effect is assessed in the present section for an easier interpretation of results.

The free-field sound pressure at any point of the array circle of radius r_x centered on the cylinder axis, thus in absence of the latter, and for the mode n of amplitude A_n , is expressed as an integral over the source circle, as

$$p_{ar}(r_x, \theta_x) = \frac{ik}{4} A_n \int_0^{2\pi} e^{in\phi} \frac{H_1^{(1)}(kr_\phi)}{r_\phi} [R_0 \cos \zeta - R \cos(\phi + \zeta - \xi)] d\phi, \quad (14)$$

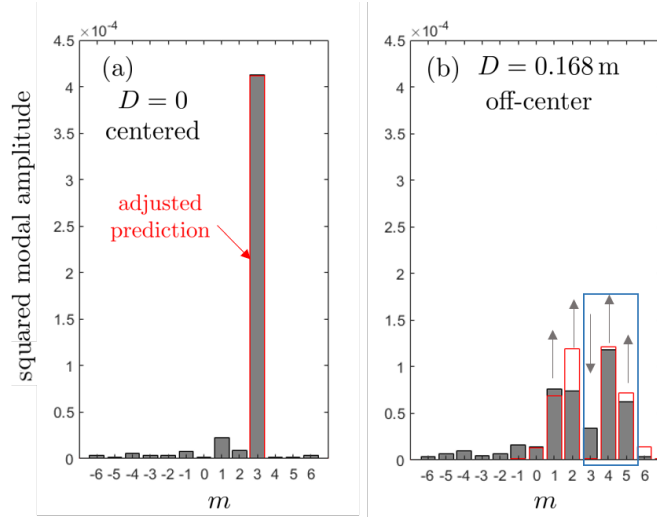


Figure 10: Measured modal structure of the free-field sound of the propeller at the BPF. High-speed case. (a): propeller at the center of the microphone array; (b): off-centered propeller. Measured values as gray bars and indicative prediction as empty red bars.

with

$$r_\phi = \sqrt{R_0^2 + R^2 - 2RR_0 \cos(\xi - \phi)},$$

if (ξ, R) denote the polar coordinates of the observer with respect to the center of the source circle (see Fig. 9). The transposition in the cylinder reference frame is ensured by the relations

$$R = \sqrt{r_x^2 + D^2 - 2Dr_x \cos \theta_x}, \quad \tan \xi = \frac{r_x \sin \theta_x}{r_x \cos \theta_x - D}.$$

For the considered mode n , the post-processing leads to the complex-valued
520 modal amplitudes

$$p_m = \frac{1}{2\pi} \int_0^{2\pi} p_{ar}(r_x, \theta_x) e^{-im\theta_x} d\theta_x. \quad (15)$$

The free-field noise of the model propeller has been also measured in the experiment, after removing the cylinder, for two positions of the propeller axis: one at the center of the array, and the other one at the location corresponding to the maximum separation $D = 0.168$ of the installed configuration (see spectra
525 in Fig. 8). For this test, the propeller-and-hub element shown in Fig. 5-a has

Table 2: Expected BLH orders s and associated Bessel-function weighting factors and spinning-mode orders n at the BPF. Effective values of the factor and expected significant s orders bold-faced.

s	-1	0	1	2	3	4	5	6
$B J_{B-s}(BM)$	neg.	$4.6 \cdot 10^{-3}$	0.065	0.62	2.87	-0.62	-0.065	$-4.6 \cdot 10^{-3}$
n	4	3	2	1	0	-1	-2	-3

been mounted alone, at the tip of a vertical bar, in order to avoid azimuthal flow distortions. The modal spectra, as produced by the microphone-array processing, are plotted as gray bars in Fig. 10. Subplots (a) and (b) refer to a propeller center-point coinciding with the center of the array and displaced
530 by $D = 0.168$ m from that center, respectively. In the first case, the mode $m = n = B = 3$ dominates the radiated field, with only a negligible contribution of other modes. This rotor-locked mode is the signature of the combined steady-loading noise and thickness noise. The result confirms that residual distortions are negligible, as expected for an axisymmetric configuration. As the propeller
535 is moved away from the array center, the same processing generates a range of modes, amongst which the modes of orders (1,2,4,5), corresponding to 3 ± 1 and, less prominently, 3 ± 2 , dominate, whereas the mode 3 is strongly reduced. Bar-graph predictions of this modal-scattering effect produced by Eqs. (14) and (15) with an arbitrary amplitude are also plotted for indicative comparison. They
540 confirm the redistribution of the mode orders. In view of the overall qualitative agreement, the procedure can be used to identify the free-field signature of the propeller in the modal expansions performed in the presence of the scattering cylinder. Similar results, not shown, have been observed at the lower rotational speed. More generally, the trend has been verified that, for the largest values of
545 D , the propeller mode n is mainly seen as the modes $m = n - 1$ and $m = n + 1$.

The radiation efficiency of steady-loading noise is a matter of blade number and tangential Mach number M . In the propeller-disk plane and in the far field, at the μ^{th} harmonic of the BPF, it is determined from the value $\mu B J_{\mu B}(\mu B M)$

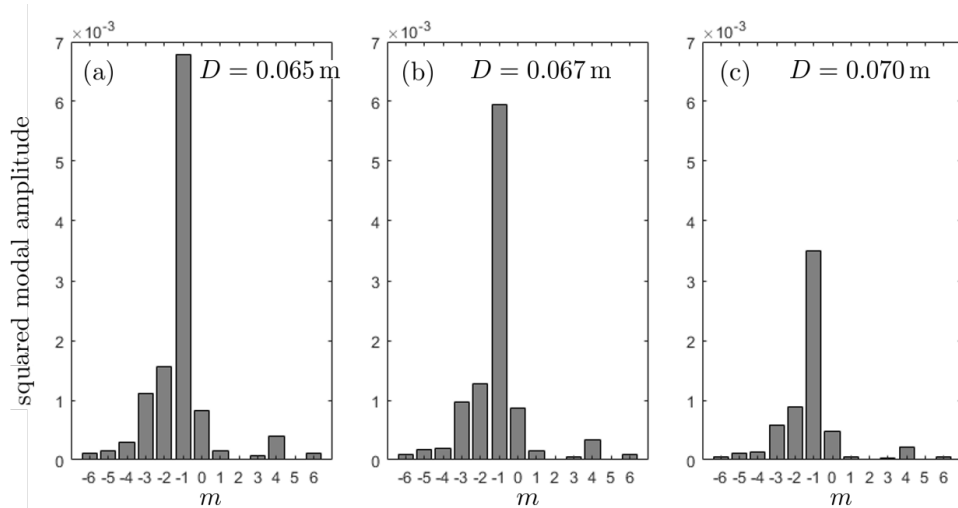


Figure 11: Measured modal structure of the total field of the installed propeller at the BPF. High-speed case, short distances D .

where B is the blade number. This value is about $4.6 \cdot 10^{-3}$ in the present case
 550 at the BPF ($\mu = 1$) and about $4.46 \cdot 10^{-5}$ at twice the BPF ($\mu = 2$). Despite its
 low but not vanishing value, the factor explains why the mode $n = B = 3$ can
 be detected in the free-field modal expansion at the BPF.

Results of the modal analysis for the installed configuration including the
 propeller and the cylinder, at the higher rotational speed, are reported in
 555 Figs. 11, 12 and 13, for the smallest, intermediate and largest axis-to-axis dis-
 tances D , respectively. In each figure, the same scale is used for the three plots.
 For small values of D (Figs. 11-a to c), a strong emergence of the mode $m = -1$
 is observed, the amplitude decreasing with increasing distance. This still holds
 for intermediate distances, as seen for instance in Fig. 12-a. Modes of orders
 560 between -3 and 0 are also found, though with much lower amplitudes. These
 negative orders are out of the range of expected BLH, as shortly discussed below
 at the light of the values in Table 2. They are attributed to cylinder scattering.

In fact, the modal analysis of the total field for varying axis-to-axis distance
 D is limited by the lack of information about actual values of the BLH. The
 565 origin of the latter lies in any distortion of the mean flow through the propeller

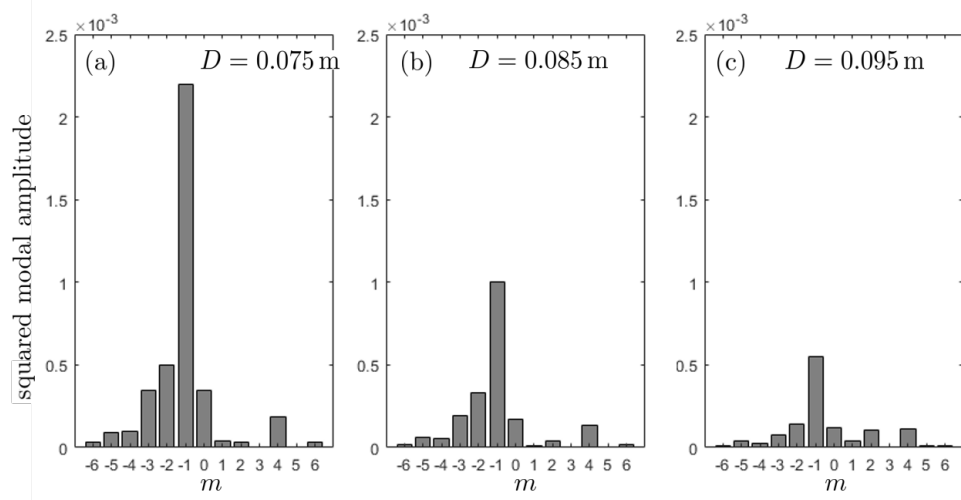


Figure 12: Measured modal structure of the total field of the installed propeller at the BPF. High-speed case, intermediate distances D .

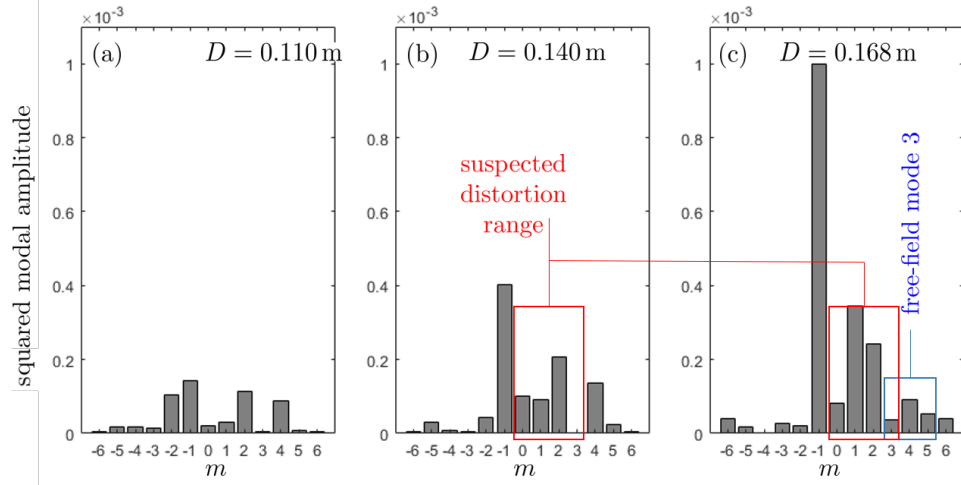


Figure 13: Measured modal structure of the total field of the installed propeller at the BPF. High-speed case, large distances D .

disk (deviation from pure axisymmetry). Their amplitudes *a priori* vary with D because the distortion is a matter of aerodynamic blockage by the cylinder. The propeller also ingests a residual wake from the sliding rods shown in Fig. 5; this contributes to the BLH. Furthermore, the amount of scattering differs for different source-mode radii. Now the radial (spanwise) distribution of the forces is unknown, which prevents from producing a quantitative analysis. Yet qualitative arguments are enough to confirm the amplification mechanism investigated in this work. Firstly, the distortions due to the vicinity of the cylinder are expected to generate low-order BLH, say typically corresponding to s between -2 and $+2$ (bold-faced values in Table 2). Secondly, as shown by Eq. (1), the weighting factor $B J_{B-s}(BM)$ involved at the BPF is significant only for small values of $|B - s|$, which leads to only retain the range of values also reported bold-faced in the second line of Table 2. Only the overlapping bold-faced ranges in the table are likely to produce a significant contribution. This suggests that, irrespective of their unknown amplitudes, the BLH of orders $s = 1, 2$ dominate in the direct field of the installed propeller, in addition to the steady-loading noise. The main effect of the off-origin positioning is to generate the modes $m = 0$ and 2 for $s = 1$ and the modes $m = 1$ and 3 for $s = 2$ in the modal expansion computed from the microphone array.

The results for the largest axis-to-axis distances, Fig. 13, seem contradictory. Indeed, the mode amplitudes increase significantly with increasing distance D , with a dominant mode -1 . The observed modes of orders $0, 1, 2$, with moderate amplitudes, are those expected from an azimuthal distortion. They are highlighted by the red boxes in Figs. 13-b and c. It is worth noting that the modes $3, 4, 5$ grouped in the blue box in Fig. 13-c have the same amplitudes as in the free-field configuration reported in Fig. 10. This suggests that the rotor-locked mode $n = 3$ in the reference frame of the propeller is still recognizable in the modal expansion. But it is of secondary importance in the total sound field. It is conjectured that the 'free-field' modes 1 and 2 in Fig. 10-b are overwhelmed by the same modes as generated by the additional distortion in the presence of the cylinder and sliding bars, in Fig. 13-c. Such a distortion could only be de-

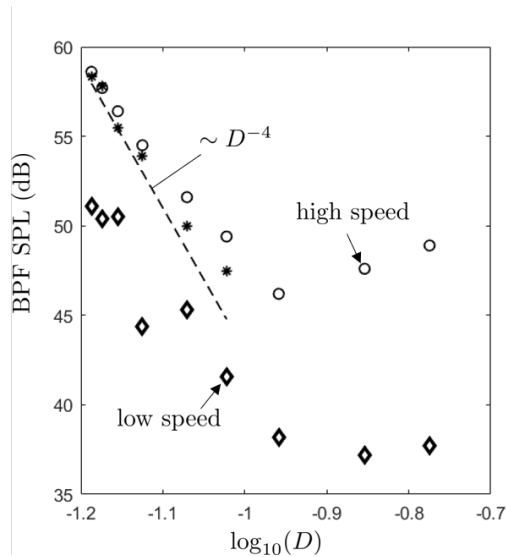


Figure 14: BPF tone level as a function of separation D , with 20-Hz bandwidth integration, for the high-speed (\circ) and low-speed (\diamond) cases. D^{-4} -law featured by the dashed line. (*): relative levels of the mode $m = -1$ from Figs. 11 and 12, shifted for comparison.

tected by advanced and non-intrusive optical techniques, well beyond the scope of the present study.

5.4. Tonal-Noise Amplification

600

The amplification rate of the BPF harmonics by the asymptotic behavior of the Green's function is finally addressed in this section. The observed variations of the tonal noise with the separation D are also compared with theoretical predictions.

605

Figure 14 displays the BPF tone level, integrated in a 20-Hz bandwidth, as a function of the separation D , for the low and high rotational speeds. A log-scale is used for D . Despite unexplained irregularities in the low-speed case for small separations (diamond symbols, \diamond), the same overall trend is found. The BPF tone levels decrease at the same rate for both speeds, for small and moderate separations D . The global difference of about 6 dB between low-speed

610

and high-speed data is expected from the scaling law of dipole sources with the sixth power of flow speed in aeroacoustics [3]. Indeed, using the rotational speed as reference, $60 \log_{10}(14800/11800) = 5.9$. Then the sound slightly increases for larger separations. The amplitudes of the mode $m = -1$ in relative decibels, as deduced from Figs. 11 and 12, are also plotted as star symbols (*), for the high-speed case. The values are shifted vertically to fit the measured tone levels (symbols \circ) at the shortest separations. Both negative slopes are close to each other, confirming that the tone level and its decrease are mostly determined by the mode $m = -1$.

If it is assumed that blade-loading harmonics are only generated at a negligible level as the propeller is moved very close to the cylinder, the modal structure of the direct sound field of the propeller is dominated by the mode $n = 3$. The amplitude of the associated scattered field is determined by the cylinder mode $m = -1$, according to Eq. (8). A sound-pressure amplitude proportional to D^{-4} is expected. This asymptotic law is reported as the dashed line in Fig. 14. The actual rate of decrease is slightly slower, suggesting that modes of orders $n \neq 3$ are also generated.

The main outcomes of the experiment are twofold. Firstly, the tonal noise at the BPF combines the rotor-locked mode $n = 3$ and a couple of adjacent modes. Secondly, these modes are dominantly scattered as the mode $n = -1$ as the propeller-cylinder distance decreases, with a strong amplification. This is expected from the present theoretical developments.

Finally, typical instantaneous pressure maps computed with the exact analytical formulation are shown in Fig. 15, in order to illustrate the features of the combined direct and scattered fields. These test cases reproduce configurations of the experiment, with the rotor-locked source-mode $n = 3$ as primary sound. The characteristic attenuation distance, over which the direct field of this mode decreases down to very low values, has the same order of magnitude as the mode radius, as suggested by the size of the six spots on the maps, one per half lobe. The separation of $D = 168$ mm, Fig. 15-a, largely exceeds the attenuation distance of the mode. Therefore, the scattered field from the cylin-

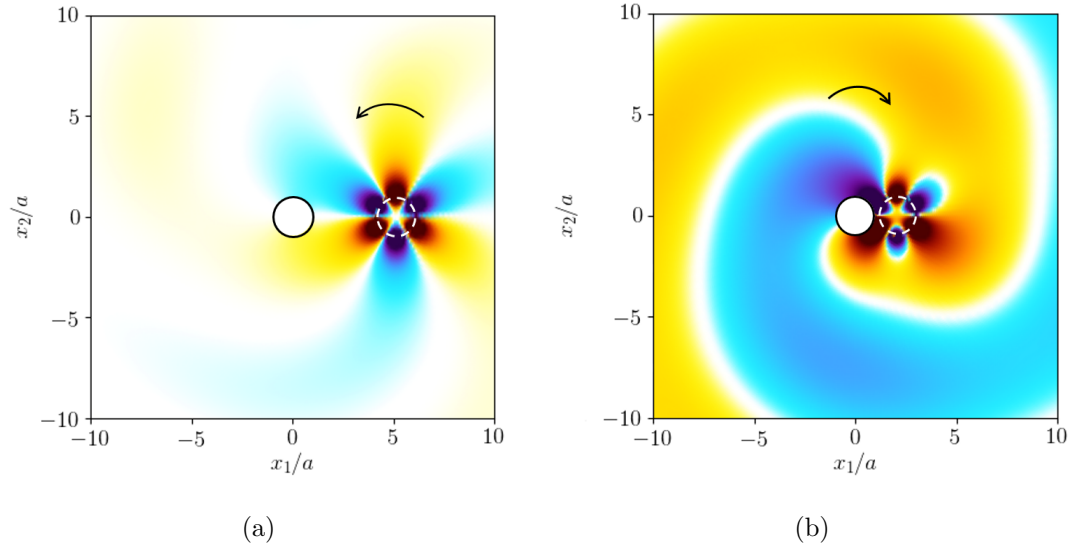


Figure 15: Predicted instantaneous pressure maps of a circular array of phased dipoles in the presence of a scattering cylinder, for the counterclockwise rotor-locked mode $n = 3$. Cases of weak scattering, $D = 168$ mm (a) and compact regime, $D = 65$ mm (b), featuring the formation of the mode $m = -1$. Parameters representative of the experiment. Source mode featured as dashed circle, same arbitrary color scale on both plots. The arrows indicate the directions of rotation of the direct mode $n = 3$ in subplot (a) and of the scattered mode $m = -1$ in subplot (b).

der is relatively weak, because of the same amplitude as the local direct field at the location of the cylinder surface. In contrast, the small separation of $D = 65$ mm, Fig. 15-b, is substantially smaller than the attenuation distance. In this case, the scattered field is of the same order of magnitude as the direct field close to its source. But because the generated mode $m = -1$ is now radiating instead of evanescent, the scattered field is much larger than the direct field at large distances. This example illustrates the amplification mechanism.

The three parameters involved in the diffraction mechanism are the distance L between the cylinder surface and the source-mode center, and the two radii a and R_0 . The analytical model based on the exact Green's function, Eq. (3) allows to investigate extended ranges of these parameters, in order to identify critical areas of amplification. Such a parametric study, covering configurations

representative of the experiment, is illustrated for the source-modes $n = 1$ and
655 $n = 3$ in Figs. 16-a and 16-b, respectively, with SPL maps. On each map, an
arbitrary decibel scale is used, so that only the variations make sense. Indeed,
the source strengths are unknown and the information of interest is the effect
of the cylinder on the radiating properties of a mode. Because the mode $n = 1$
already radiates efficiently in free field, cylinder scattering only induces moder-
660 ate modifications on it. As a result, the map in Fig. 16-a exhibits variations of
about 1 dB.

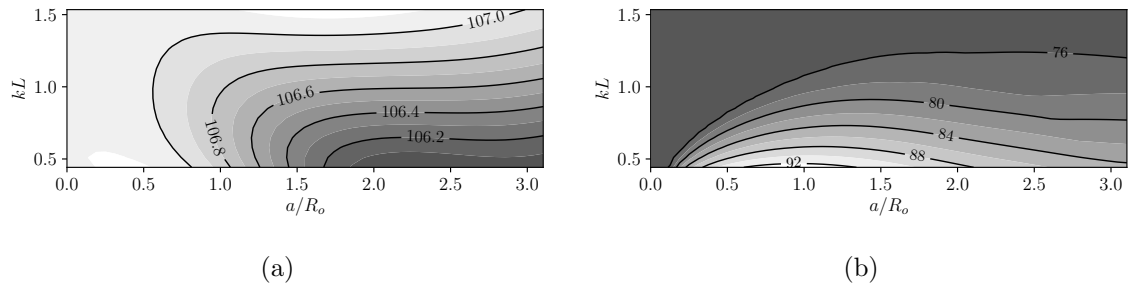


Figure 16: Total-field SPL maps of individual source-modes in arbitrary decibel scale, as a function of the distance L between cylinder edge and source-mode center and of the ratio a/R_0 . $kR_0 = 0.44$; modes $n = 1$ (a) and $n = 3$ (b). Parameters representative of the experiment.

In contrast, the mode $n = 3$ is evanescent in free field and experiences strong amplification by asymptotic cylinder scattering. The map in Fig. 16-b now exhibits large variations. The SPL increases as the source-mode to cylinder
665 distance L is reduced. Two other important conclusions can be drawn. Firstly, the SPL drops for $a \ll R_0$, which means that the amplification no longer operates for vanishing cylinder size. Secondly, a maximum amplification regime is found for $a/R_0 \simeq 1$. These important features could be the basis for the definition of guidelines when designing a global architecture.

670 6. Application to Hub Scattering

The scattering effect of the hub or the center body of a propeller on the emitted tonal noise has been pointed out in air by various authors [20, 21, 22, 23].

The question also arises for the hub of marine propellers, in connection with the possible amplification effect inherent to the compact regime. It is answered in this section, with a straightforward application of the exact analytical model of sections 3 and 4, in the special case of coaxial cylinder and source-mode, as depicted in Fig. 17. The generic configuration of Fig. 1 is simply reconsidered by setting $D = 0$, so that the source-mode component of propeller tonal noise is centered at the origin of the cylinder coordinates (r_x, θ_x) , with the condition $R_0 > a$. The same compactness conditions $kR_0 \ll 1$ and $ka \ll 1$ are again assumed. The same exact analytical computations and source-mode discretization procedure are applied.

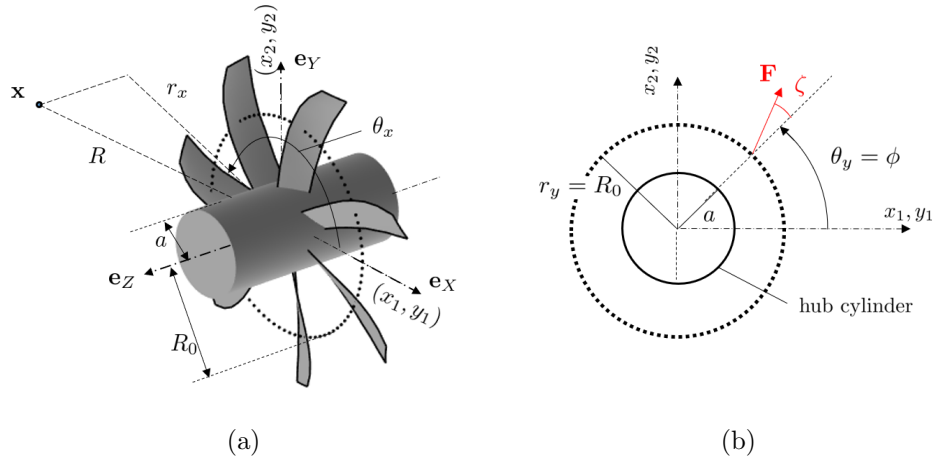


Figure 17: Coordinates and main notations for coaxial source-mode and scattering cylinder. (a): three-dimensional propeller-and-hub configuration, (b): two-dimensional reduction, featuring the source-mode as dotted-line circle. Note that $D = 0$ with respect to Fig. 2.

The effect of center-body scattering on the amplitude of the radiated field is assessed by averaging the far-field sound pressure for all observation angles, and by comparing it to the free-field radiation. The result is reported for various mode orders in Fig. 18, where the Sound Pressure Level difference ΔSPL is plotted as a function of the ratio a/R_0 , for a fixed value of ka . The radiated sound is found to increase as the sources get closer to the cylinder surface, for the same assumed dipole strength. For any mode order, the sound increase reaches

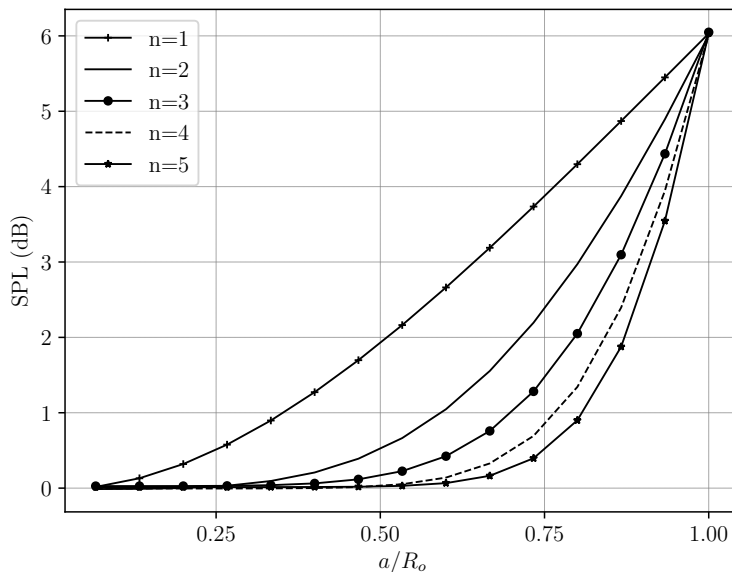


Figure 18: Averaged far-field Sound Pressure Level radiated by various source-mode orders n in the presence of a hub, as a function of a/R_0 . $ka = 0.10$.

+6 dB as the source-mode radius approaches the hub radius, $a/R_0 \sim 1$. This result is intuitively expected by similarity with the image principle, according to which sources approaching a rigid plane have their radiated sound pressure doubled. It is also recovered by an asymptotic analysis of the Green's function, considering $D = 0$ with the following set of conditions:

$$kr_x \gg 1, ka \ll 1, kR_0 \ll 1, aR_0 \sim 1.$$

Following the same procedure as in section 4, the asymptotic derivations, not further detailed, are made substantially simpler because the sources are centered, leading to $r_y = R_0$ and $\theta_y = \phi$. The point dipole of angular coordinate ϕ along the source circle is the same for radial and tangential forces, and it is expressed as $F_s^R, F_s^T \propto e^{in\phi}$. Finally, the leading order of the total field is obtained as

$$p_{1as}(r_x, \theta_x) = 2p_{0as}(r_x, \theta_x),$$

which is consistent with the exact analytical model. This maximum amount

of sound-pressure increase remains well below the amplification evidenced in
685 previous sections for off-axis source-modes. In that sense, hub scattering is free
of true amplification, which can be interpreted as follows. The amplification
by compact Green's function behavior is typical of higher-order source-modes.
Because the latter are compact distributions of dipoles with zero instantaneous
balance, they have at most a quadrupole-like efficiency in free field, by virtue
690 of partial cancellation. Any off-centered scattering body in compact vicinity of
a source-mode generates very different elementary scattered fields for the con-
stitutive point dipoles. This imbalance makes the resulting partial cancellation
much less pronounced, thus the radiation much more effective: in fact, the mode
radiates with the basic dipole-like efficiency. The situation is different for an
695 axisymmetric center body because the amount of scattering is the same for all
constitutive elements of a source-mode, leading to zero imbalance. As a re-
sult, the at-most quadrupole-like behavior is preserved, and the total-reflection
increase of 6 dB is the maximum expected effect.

7. Conclusion

700 A simple, two-dimensional analytical formulation has been implemented to
highlight fundamental aspects, that are expected to dominate the tonal noise
radiated by a marine propeller installed close to a scattering hull. For mathemat-
ical tractability, a rigid cylinder has been selected as generic hull geometry. The
formulation is based on the Green's function of the cylinder for the Helmholtz
705 equation, on the one hand, and on the notion of source-modes, on the other
hand. The source-modes are circular distributions of phased sources, repro-
ducing the free-field, or direct, radiation modes of rotor tonal noise. They are
defined in the reference frame of the propeller by their integer orders, equal to
their numbers of angular periods. In a real configuration, the direct modes are a
710 consequence of the operation of the propeller in the mean-flow distortion around
the hull. The scattered field can also be described in terms of modes, defined in the
reference frame of the cylinder. In view of the extremely low Mach numbers in

marine applications, the mean relative axial fluid motion is neglected, in both the free-field and installed radiation models. The effect of the flow distortion is concentrated in the definition of the direct modes. Furthermore, because of the very low Helmholtz numbers based on the size of a domain encompassing the source-modes and the scattering cylinder cross-section, an asymptotic regime of diffraction is encountered. This is why an asymptotic formulation has been compared to the exact calculations to interpret the results. The analytical approach provides a detailed insight into the physics of sound scattering, mode by mode. Quite generally, direct modes of higher orders (larger than 1) are found to only generate evanescent waves in free field, whereas they experience a very strong amplification in close vicinity of the cylinder. This amplification results from the interaction of the near field of the sources with the cylinder. The most spectacular result is that it generates the scattered radiating mode or order 1, whatever the direct mode order is, with inversion of the phase rotation. In contrast, the direct mode of order 1 is already very efficient in free field, because of its compactness, and only experiences a moderate amount of diffraction. The symmetric mode of order 0 radiates negligible sound, both in free-field and in the presence of the cylinder, according to the two-dimensional model.

A small-scale experiment has also been carried out in air, only based on acoustic measurements, with Helmholtz numbers representative of marine applications. For this, a three-bladed model propeller and a rigid cylinder of characteristic diameters of about 60 mm were selected, the blade passing frequency being around 750 Hz. The tests were performed in an anechoic chamber with variable relative positions, resorting to a circular array of far-field microphones to get access to the direct and scattered angular modes. The experiment clearly confirmed the amplification mechanism and the emergence of the contra-rotating mode of order 1.

The main outcomes suggest that the short distance of marine propellers to the hull of a ship could result in a dramatic acoustic installation effect, that cannot be neglected and should be taken into account at the early stage of a global design approach. The features and amplitude of the scattered field

are found very sensitive to all involved parameters, such as direct mode orders,
745 relative propeller-cylinder distance and so on. Up to that point, the simple tools
proposed in this work are well suited to investigate primary effects in a very fast
way. The theoretical study will be extended to more realistic configurations in a
future work, by resorting to a numerical determination of the Green's function
tailored to arbitrary hull geometry as proposed by Chaillat *et al.* [24].

750 **Acknowledgements** - This work was supported by Naval Group and the
LABEX CeLyA (ANR-10-LABX-0060) of *Université de Lyon*, within the pro-
gram *Investissements d'Avenir* (ANR-11-IDEX-0007) operated by the French
National Research Agency (ANR).

Declaration of competing interest - The authors declare that they have
755 no known competing financial interests or personal relationships that could have
appeared to influence the work reported in this paper.

References

- [1] J. F. Williams, D. Hawkings, Sound generation by turbulence and surfaces
in arbitrary motion, *Philosophical Transactions of the Royal Society of*
760 *London A* (264) (1969).
- [2] J. FfowcsWilliams, D. Hawkings, Theory relating to the noise of rotating
machinery, *Journal of Sound and Vibration* 10 ((1)) (1969) 10–21.
- [3] M. Goldstein, *Aeroacoustics*, McGraw-Hill Book Company, New York,
1976.
- 765 [4] F. Farassat, The derivation of a thickness noise formula for the far-field by
isom, *Journal of Sound and Vibration* 64 (1979) 159–160.
- [5] Y. Wei, YangShen, S. Jin, P. Hub, R. Lan, S. Zhuang, D. Liu, Scattering

effect of submarine hull on propeller non-cavitation noise, *Journal of Sound and Vibration* 370 (2016) 319–335.

- 770 [6] C. Testa, L. Greco, Prediction of submarine scattered noise by the acoustic analogy, *Journal of Sound and Vibration* 426 (2018) 186–218.
- [7] M. Roger, K. Kucukcoskun, Near-and-far field modeling of advanced tail-rotor noise using source-mode expansions, *Journal of Sound and Vibration* 453 (2019) 323–354.
- 775 [8] A. Carazo, M. Roger, M. Omais, Analytical prediction of wake-interaction noise in counter-rotating open rotors, 17th AIAA/CEAS, Aeroacoustics Conference (2011).
- [9] M. S. Howe, Sound generation in a fluid with rigid boundaries, in: *Acoustics of Fluid-Structures Interactions*, Cambridge, 1998, p. 164–166.
- 780 [10] J. E. Ffowcs Williams, L. H. Hall, Aerodynamic sound generation by turbulent flow in the vicinity of a scattering half-plane, in: *Journal of Fluids Mechanics*, 1970.
- [11] M. Roger, S. Moreau, K. Kucukcoskun, On sound scattering by rigid edges and wedges in a flow, with applications to high-lift device aeroacoustics, 785 *Journal of Sound and Vibration* 362 (2016) 253–275.
- [12] M. Goldstein, Unified approach to aerodynamic sound generation in the presence of solid boundaries, *Journal of the Acoustical Society of America* (1974) 497–509.
- 790 [13] D. B. Hanson, D. J. Parzych, Theory for noise of propellers in angular in- flow with parametric studies and experimental verificatio, Final Report United Technologies Corp., Windsor Locks, CT. Standard Div., vol. 1 (1993).
- [14] M. Abramowitz, I. Stegun, *Handbook of mathematical functions*, DOVER, New-York, US, 1970.

- 795 [15] M. Roger, Near-field fan noise modelling and installation effects due to scattering surfaces, *Fan Noise 2007* (2007).
- [16] P. M. Morse, K. U. Ingard, *Theoretical Acoustics*, Princeton University Press, Princeton, New Jersey, 1986.
- [17] X. Gloerfelt, F. Pérot, C. Bailly, D. Juvé, Flow-induced cylinder noise formulated as a diffraction problem for low mach numbers, *Journal of Sound and Vibration* 287 (2005) 129–151.
- 800 [18] I. S. Gradshteyn, I. M. Ryzik, *Tables of integrals, series and products*, Academic Press, New-York, US, 1980.
- [19] M. Whatmore, A.R. & Lowson, Some effects of ground and side planes on the acoustic output of a rotor, *NASA CR-132306* (1973).
- 805 [20] A. Parry, D. Crighton, Asymptotic theory of propeller noise—part i: Subsonic single-rotation propeller, *AIAA Journal* 29 (1991) 2031–2037.
- [21] M. Kingan, R. Self, Open rotor tone scattering, *Journal of Sound and Vibration* 331 (2012) 1806–1828.
- 810 [22] S. Glegg, Effect of centerbody scattering on propeller noise, *AIAA Journal* 29 (1991) 572–576.
- [23] M. Kingan, P. S. Institute, Open rotor centrebody scattering, *Journal of Sound and Vibration* 333 (2014) 418–433.
- [24] S. Chaillat, B. Cotté, J.-F. Mercier, G. Serres, N. Trafny, Efficient evaluation of three-dimensional helmholtz green’s functions tailored to arbitrary rigid geometries for flow noise simulations, *Journal of Computational of Physics* 452 (2022).
- 815